Towards Continuous-Variable Quantum Convolutional Networks for Biomedical Imaging

Authors
M.Sc. Daniel Alejandro Lopez Montiel
Dr. Oscar Humberto Montiel Ross
Dr. Miguel Ángel Lopez Montiel
Dr. Oscar Castillo

October 21st, 2025

Content

1.- Introduction

AI for Medical Imaging: Progress and Limitations

- AI, has revolutionized medical image analysis [1–3].
- However, these models rely on **large datasets and heavy computation**, limiting their scalability and interpretability [4].
- **Quantum computing** emerges a new paradigm to process information more efficiently [5].

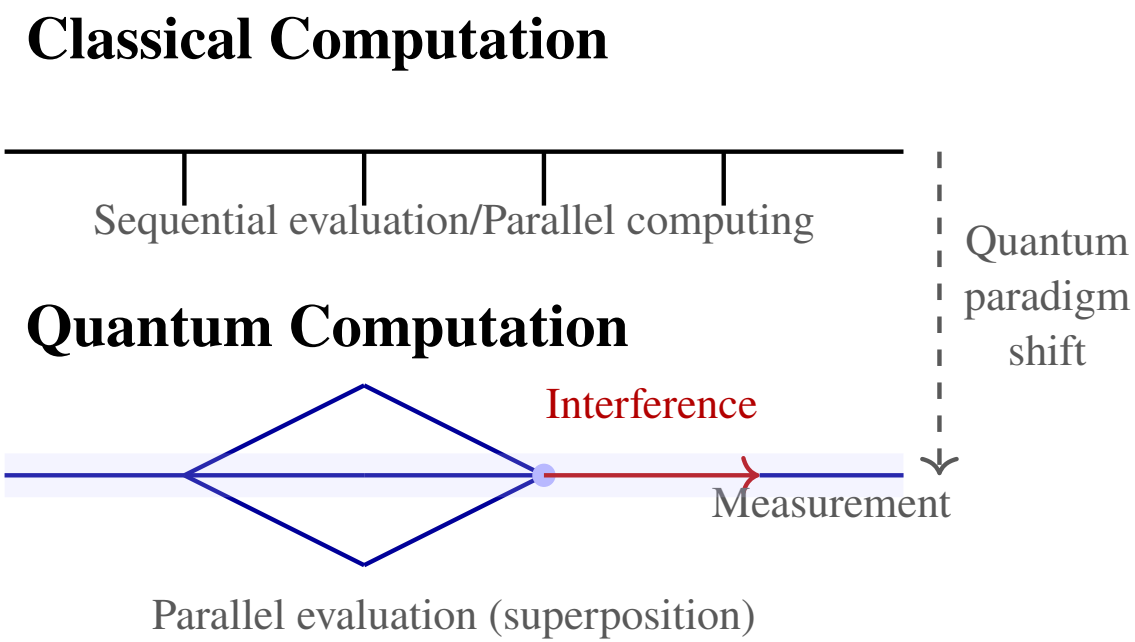

Figure 1: Computation paradigm features and shift.

Quantum AI: Paradigms and Gaps

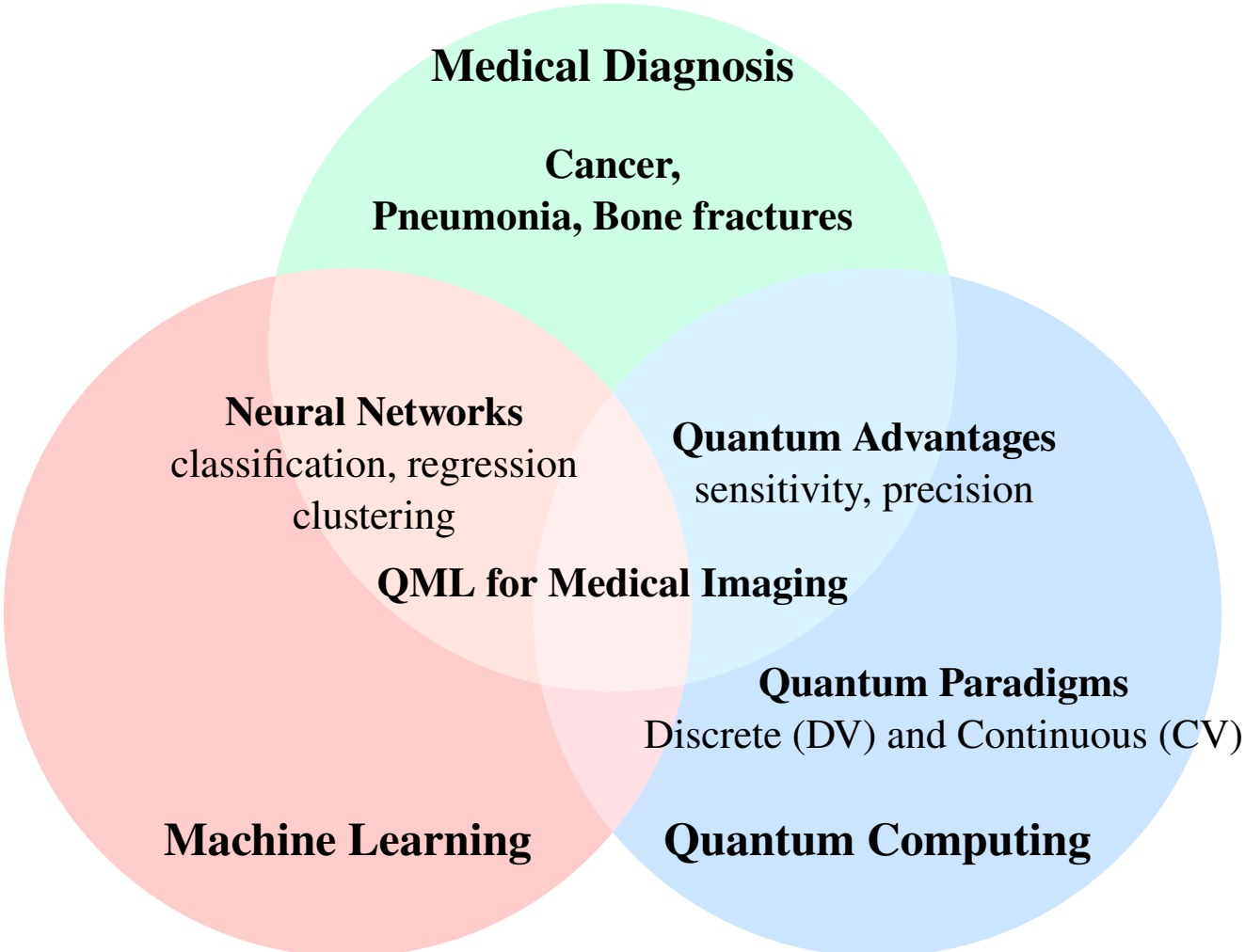

Figure 2: Intersection of disciplines highlighting the research gap in quantum-enhanced medical diagnosis.

Our proposal

- Explore **CV-QNNs** for medical image classification.
- Use **Gaussian gates** (D, R, S, BS) to emulate convolutional behavior.
- Evaluate model performance, robustness, and expressiveness against classical and DV quantum counterparts.

Datasets: BreastMNIST, OrganAMNIST, PneumoniaMNIST
Evaluation: Accuracy, F1-score, AUROC, noise robustness, interpretability.

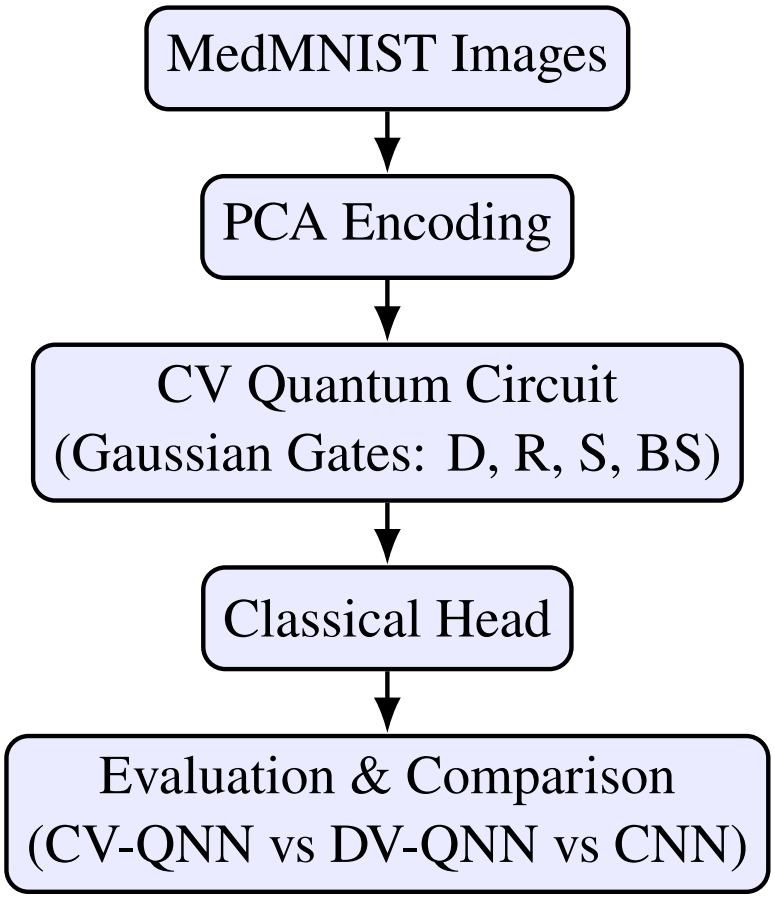

Figure 3: Methodology of the proposed work.

2.- Related work

State-of-the-art of Continuous-Variable QML

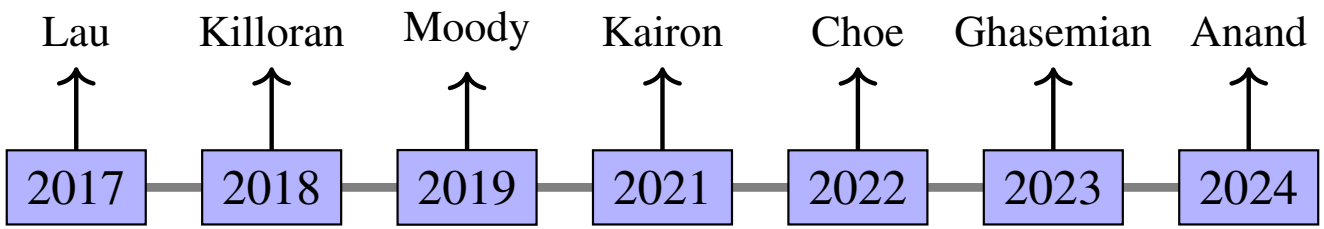

Figure 4: Recent state-of-the-art of Continuous-Variable QML.

State-of-the-art of Continuous-Variable QML

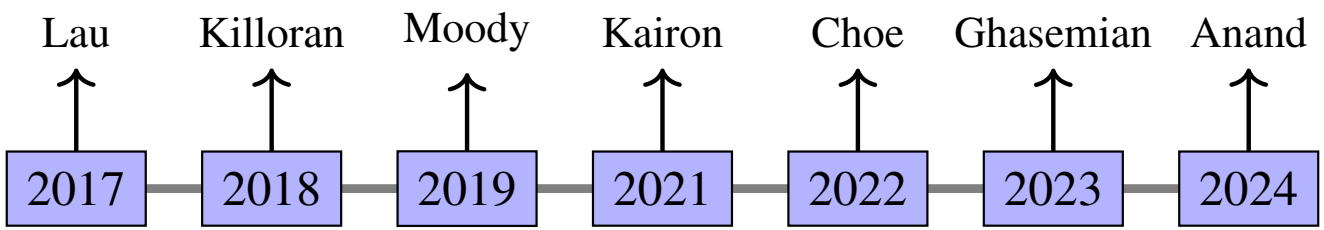

Figure 4: Recent state-of-the-art of Continuous-Variable QML.

- **2017:** Subroutines are generalized for infinite-dimensional systems [6].

State-of-the-art of Continuous-Variable QML

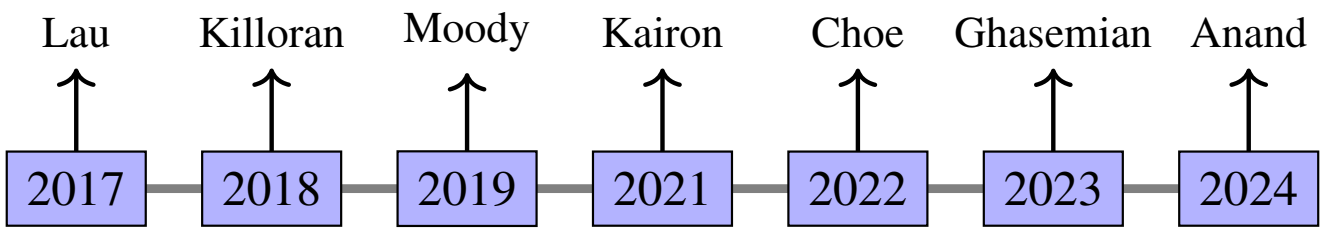

Figure 4: Recent state-of-the-art of Continuous-Variable QML.

- **2017:** Subroutines are generalized for infinite-dimensional systems [6].
- **2018:** First CV neural networks for CV quantum computers [7].

State-of-the-art of Continuous-Variable QML

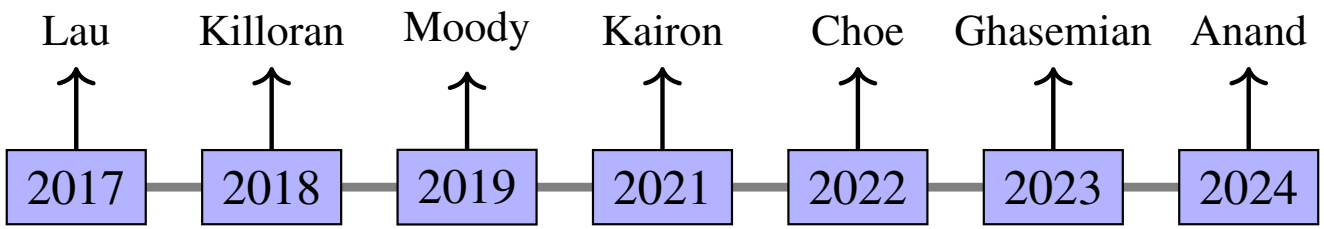

Figure 4: Recent state-of-the-art of Continuous-Variable QML.

- **2017:** Subroutines are generalized for infinite-dimensional systems [6].
- **2018:** First CV neural networks for CV quantum computers [7].
- **2019:** ML and optimization with variable parameters for short-depth photonic circuits [8].

State-of-the-art of Continuous-Variable QML

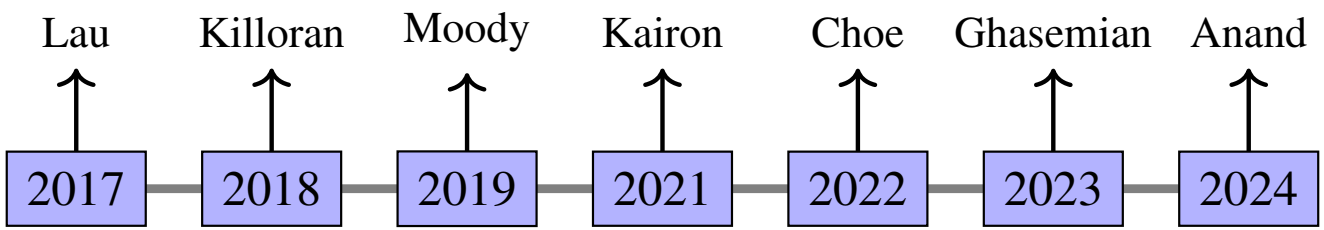

Figure 4: Recent state-of-the-art of Continuous-Variable QML.

- **2017:** Subroutines are generalized for infinite-dimensional systems [6].
- **2018:** First CV neural networks for CV quantum computers [7].
- **2019:** ML and optimization with variable parameters for short-depth photonic circuits [8].
- **2021:** COVID-19 diagnosis through CV QNNs [9].

State-of-the-art of Continuous-Variable QML

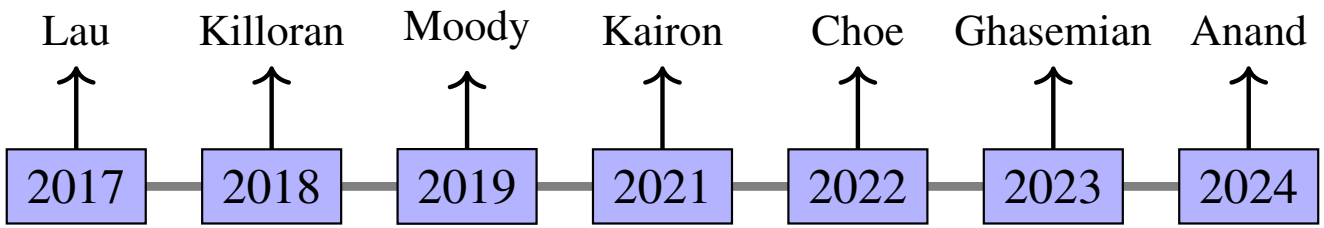

Figure 4: Recent state-of-the-art of Continuous-Variable QML.

- **2017:** Subroutines are generalized for infinite-dimensional systems [6].
- **2018:** First CV neural networks for CV quantum computers [7].
- **2019:** ML and optimization with variable parameters for short-depth photonic circuits [8].
- **2021:** COVID-19 diagnosis through CV QNNs [9].
- **2022:** MNIST classification via CV QNN architecture [10].

State-of-the-art of Continuous-Variable QML

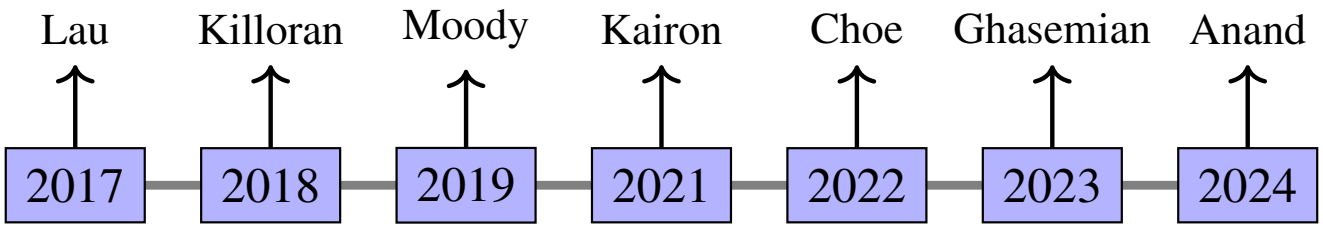

Figure 4: Recent state-of-the-art of Continuous-Variable QML.

- **2017:** Subroutines are generalized for infinite-dimensional systems [6].
- **2018:** First CV neural networks for CV quantum computers [7].
- **2019:** ML and optimization with variable parameters for short-depth photonic circuits [8].
- **2021:** COVID-19 diagnosis through CV QNNs [9].
- **2022:** MNIST classification via CV QNN architecture [10].
- **2023:** Neural network implementations on photonic computers to encode spectral amplitude information [11].

State-of-the-art of Continuous-Variable QML

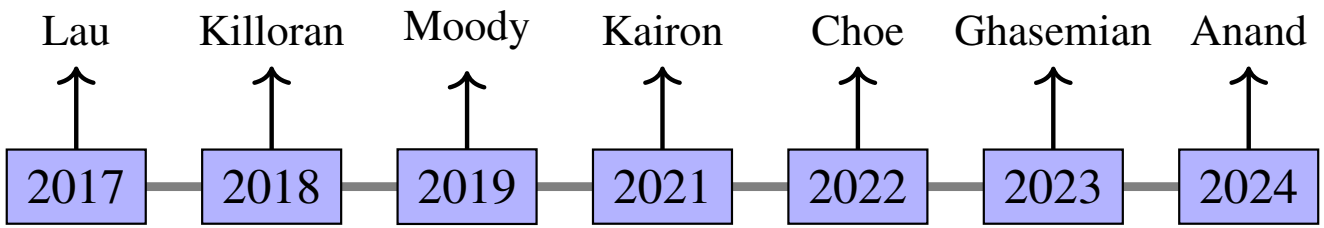

Figure 4: Recent state-of-the-art of Continuous-Variable QML.

- **2017:** Subroutines are generalized for infinite-dimensional systems [6].
- **2018:** First CV neural networks for CV quantum computers [7].
- **2019:** ML and optimization with variable parameters for short-depth photonic circuits [8].
- **2021:** COVID-19 diagnosis through CV QNNs [9].
- **2022:** MNIST classification via CV QNN architecture [10].
- **2023:** Neural network implementations on photonic computers to encode spectral amplitude information [11].
- **2024:** Time-series forecasting comparison between quantum CV, DV and classical approaches [12].

3.- Methodology

Data preparation

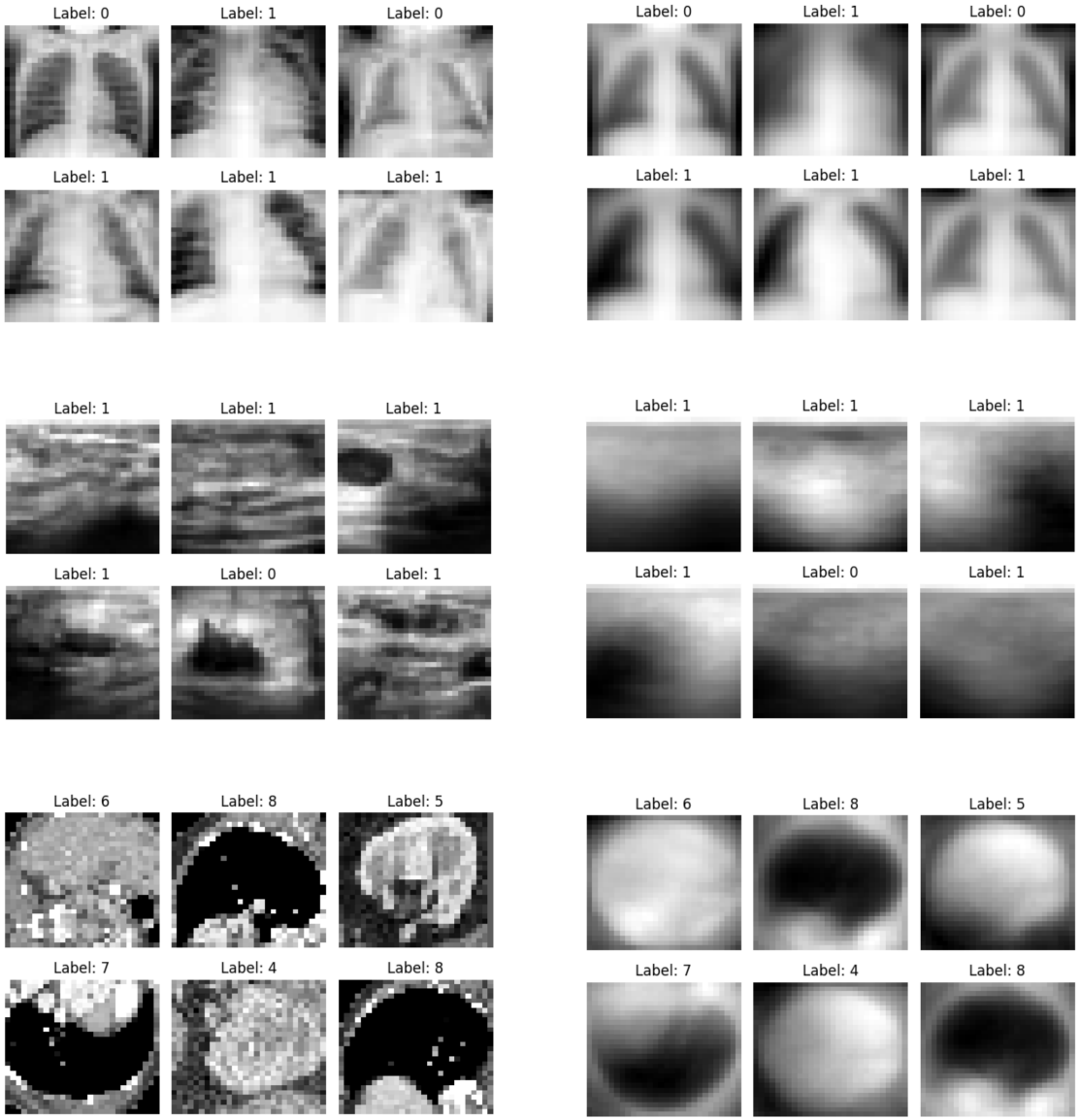

Figure 5: Comparison between original and PCA-reconstructed images.

Data dimensionality reduction

Table 1: Dimensionality reduction using PCA across MedMNIST datasets.

Dataset	**Task**	**Dimensions**	**No. Samples**	**PCA**	σ^2
Breast	Binary	(28, 28, 1)	546	4	~60%
Organ	Multiclass	(28, 28, 1)	10368	4	~48%
Pneumonia	Binary	(28, 28, 1)	4708	4	~60%

Continuous-Variable quantum neural network

Continuous-Variable quantum neural network

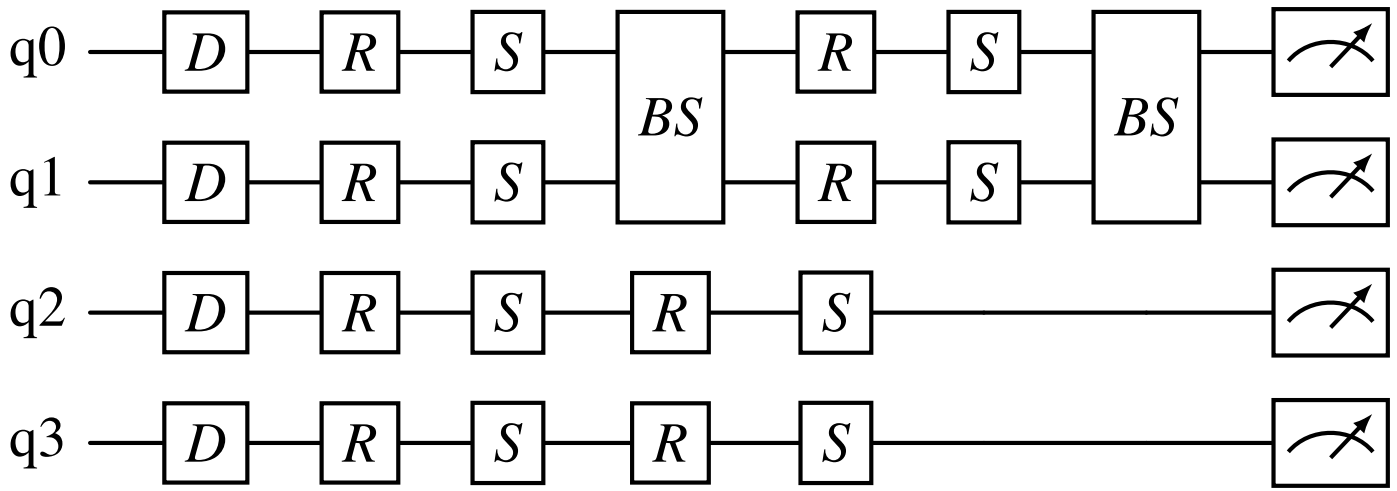

Figure 6: The proposed 4-mode Continuous-Variable (CV) quantum circuit.

Displacement gate

$$D(\alpha) = \exp\left(\alpha \hat{a}^{\dagger} - \alpha \hat{a}\right), \tag{1}$$

Continuous-Variable quantum neural network

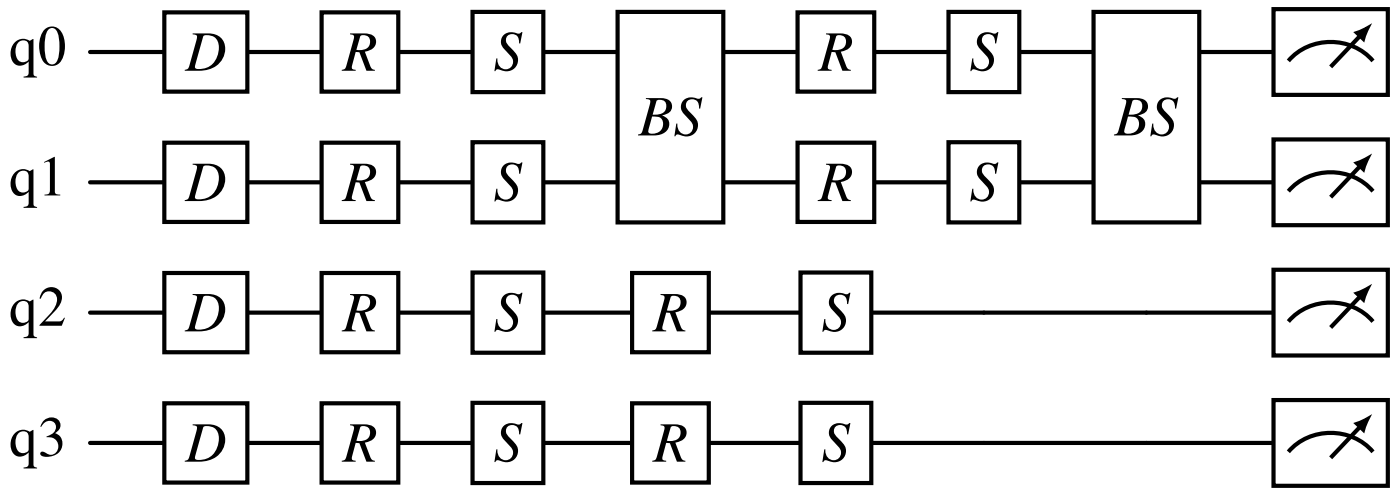

Figure 6: The proposed 4-mode Continuous-Variable (CV) quantum circuit.

Rotation gate

$$R(\phi) = \exp\left(i\phi\hat{a}^{\dagger}\hat{a}\right), \tag{2}$$

Continuous-Variable quantum neural network

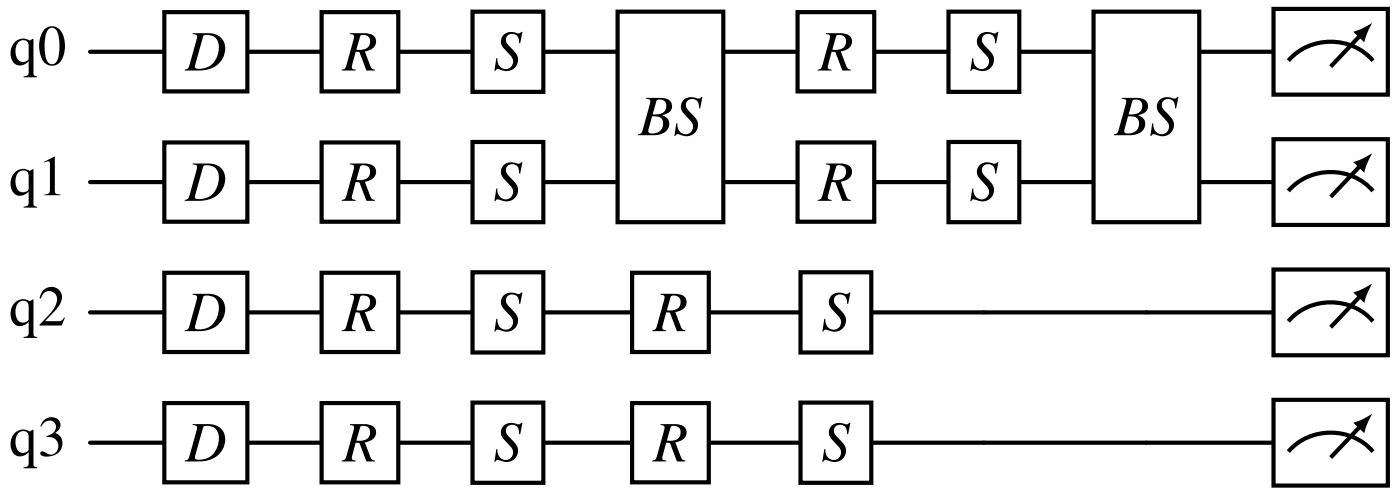

Figure 6: The proposed 4-mode Continuous-Variable (CV) quantum circuit.

Squeezing gate

$$S(r) = \exp\left[\frac{1}{2}r\left(\hat{a}^2 - (\hat{a}^\dagger)^2\right)\right], \tag{3}$$

Continuous-Variable quantum neural network

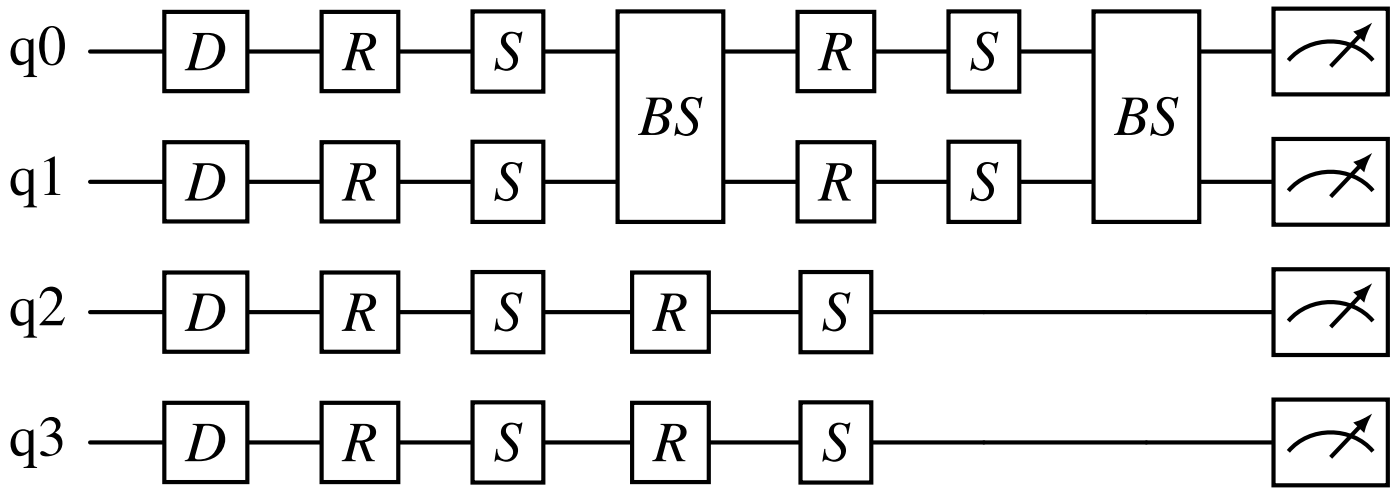

Figure 6: The proposed 4-mode Continuous-Variable (CV) quantum circuit.

Beamsplitter gate

$$BS(\theta, \phi) = \exp\left[\theta\left(e^{i\phi}\hat{a}_1^\dagger \hat{a}_2 - e^{-i\phi}\hat{a}_1 \hat{a}_2^\dagger\right)\right], \tag{4}$$

Continuous-Variable quantum neural network

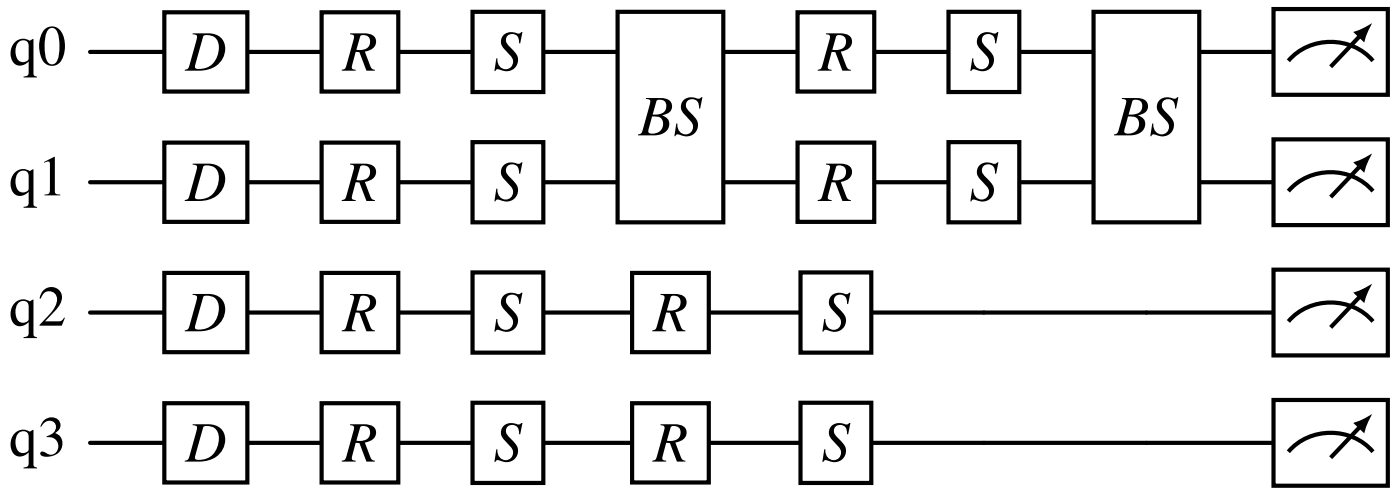

Figure 6: The proposed 4-mode Continuous-Variable (CV) quantum circuit.

Measurement on position quadratures

$$\mathbf{y} = \left[\langle \hat{X}_1 \rangle, \langle \hat{X}_2 \rangle, \ldots, \langle \hat{X}_n \rangle \right]. \tag{5}$$

Continuous-Variable quantum neural network

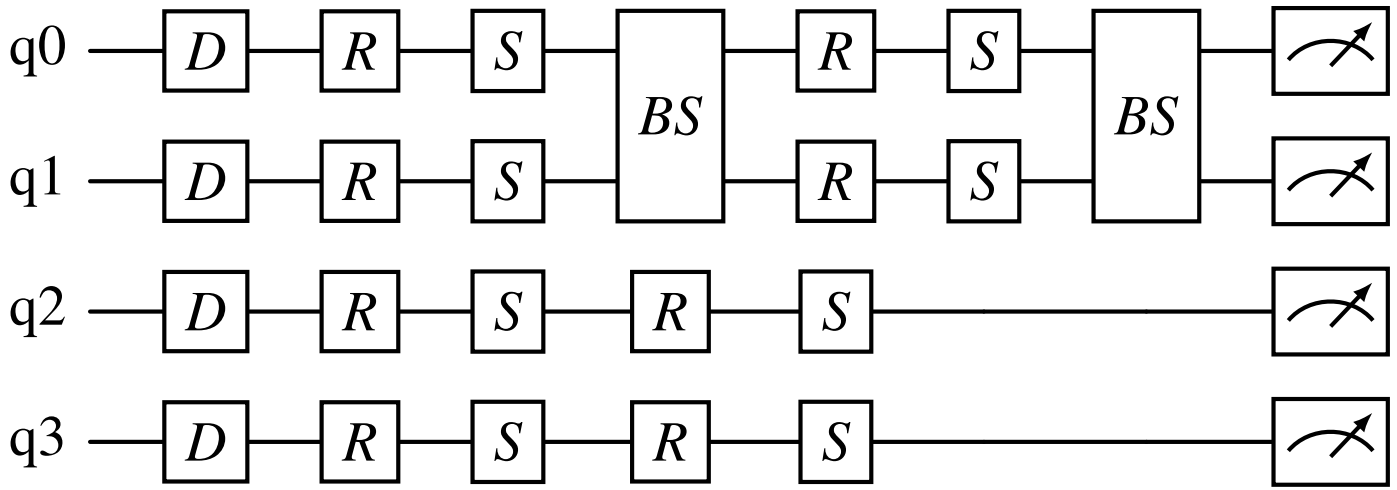

Figure 6: The proposed 4-mode Continuous-Variable (CV) quantum circuit.

Component	**Formula**	**Parameters**	**Description**
Quantum CV Layer	$2 \times 4 \times 4$	32	(D, R, S, BS)
Classical Head	$4 \times 2 + 2$	10	Linear layer mapping
Total	–	**42**	Trainable parameters

Discrete-Variable quantum neural network

Discrete-Variable quantum neural network

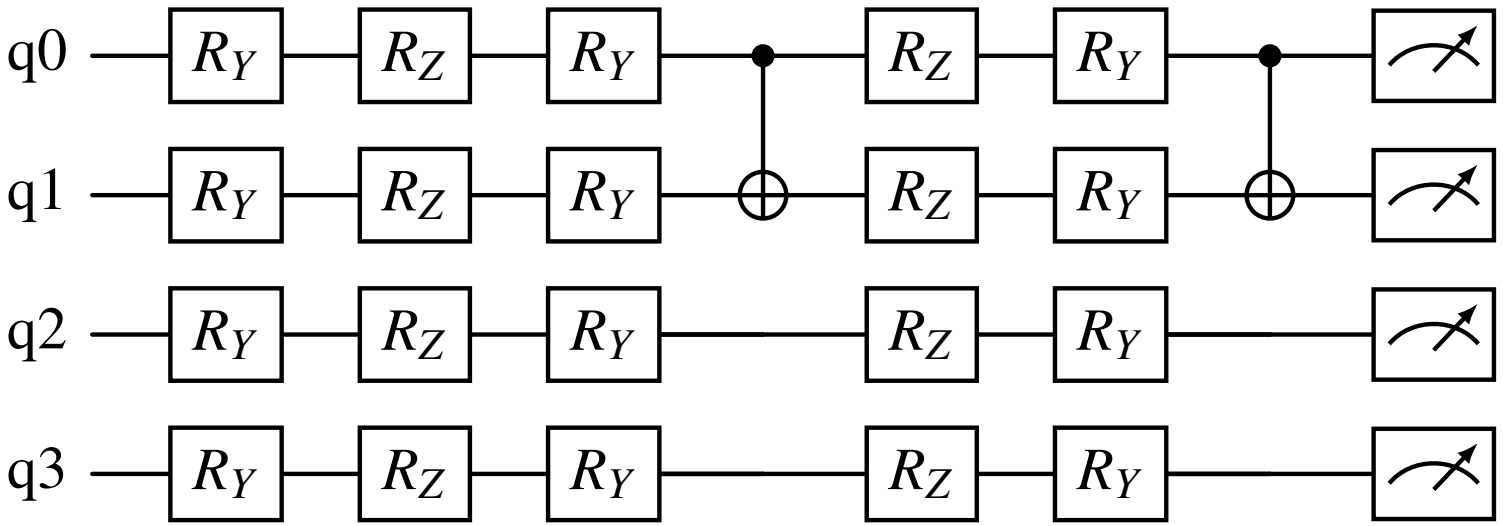

Figure 7: The proposed 4-qubit DV quantum circuit.

Rotation on y-axis gate

$$R_y(\phi) = e^{-i\phi\sigma_y/2} = \begin{bmatrix} \cos(\phi/2) & -\sin(\phi/2) \\ \sin(\phi/2) & \cos(\phi/2) \end{bmatrix}, \tag{6}$$

Discrete-Variable quantum neural network

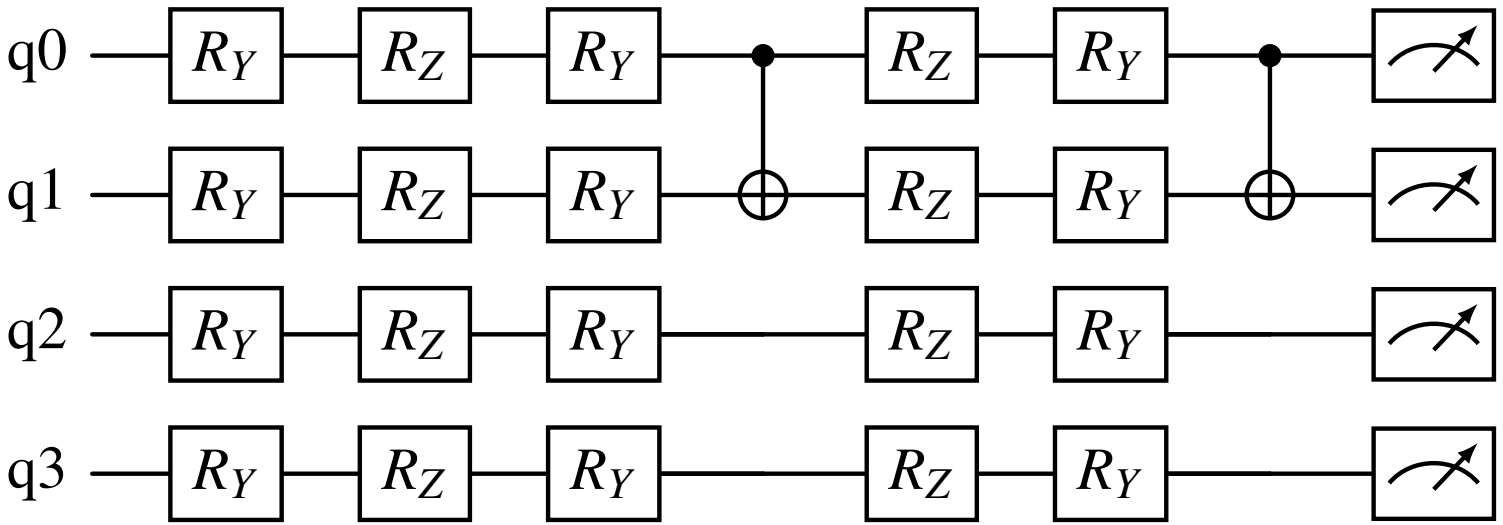

Figure 7: The proposed 4-qubit DV quantum circuit.

Rotation on z-axis gate

$$R_z(\phi) = e^{-i\phi\sigma_z/2} = \begin{bmatrix} e^{-i\phi/2} & 0 \\ 0 & e^{i\phi/2} \end{bmatrix}. \tag{7}$$

Discrete-Variable quantum neural network

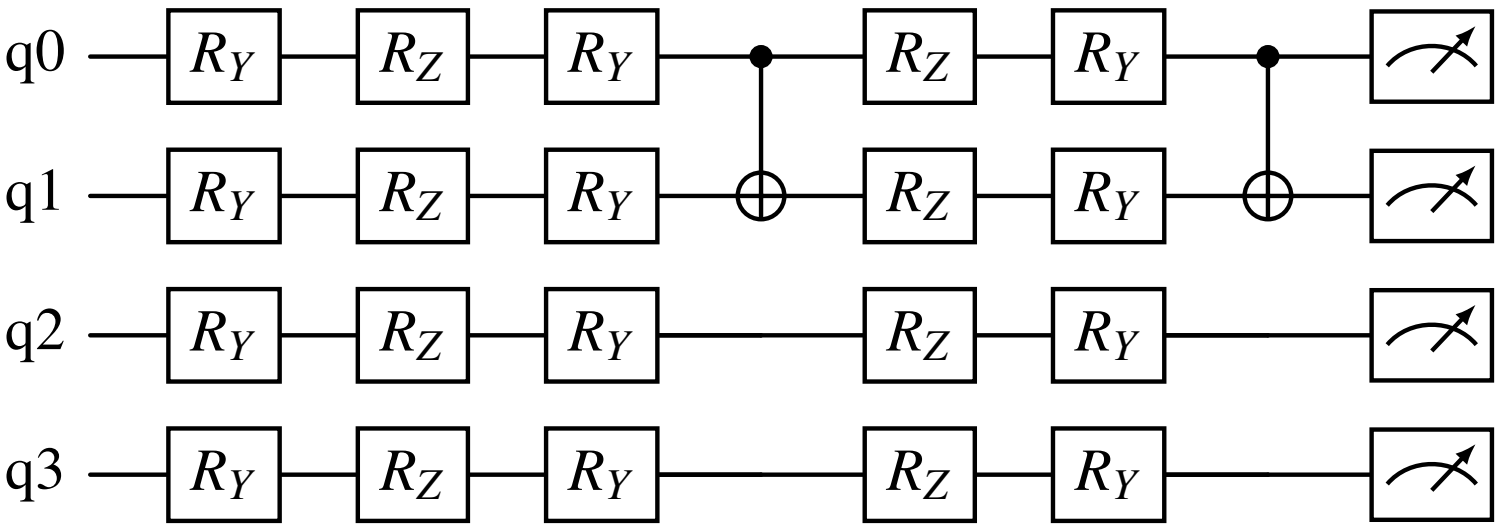

Figure 7: The proposed 4-qubit DV quantum circuit.

Controlled NOT gate

$$\text{CNOT} = |0\rangle\langle 0| \otimes I + |1\rangle\langle 1| \otimes X = \begin{bmatrix} 1 & 0 & 0 & 0 \\ 0 & 1 & 0 & 0 \\ 0 & 0 & 0 & 1 \\ 0 & 0 & 1 & 0 \end{bmatrix}. \tag{8}$$

Discrete-Variable quantum neural network

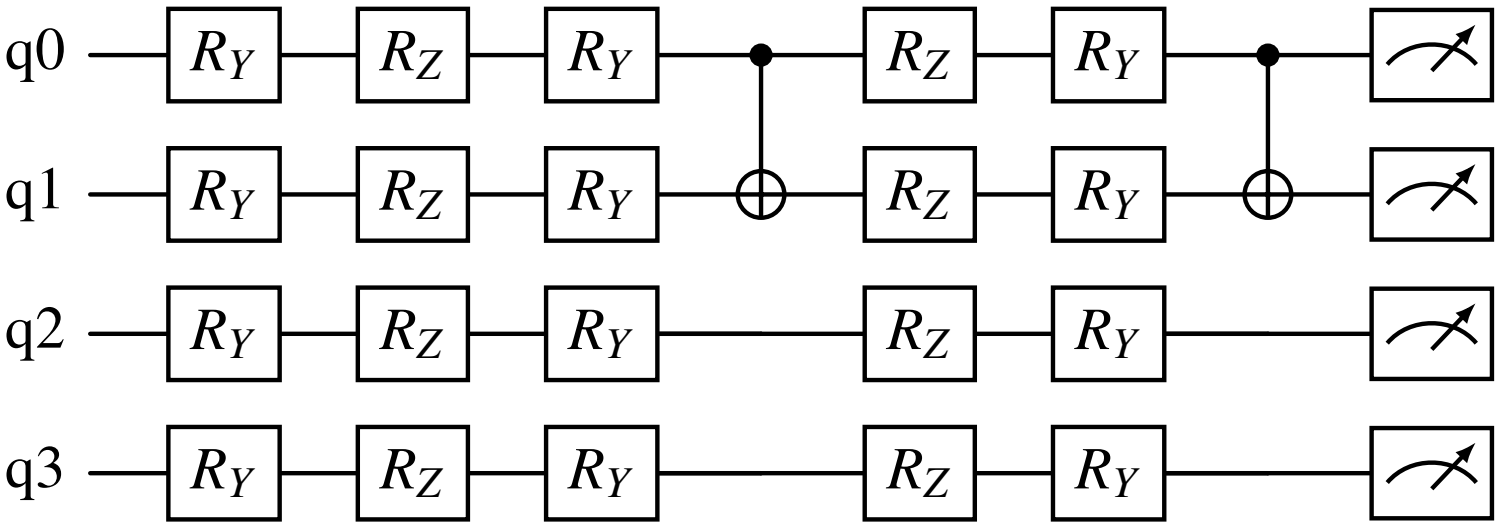

Figure 7: The proposed 4-qubit DV quantum circuit.

Measurement along the z-axis

$$\text{Measurement} = \langle\psi|\sigma_z|\psi\rangle, \tag{9}$$

Discrete-Variable quantum neural network

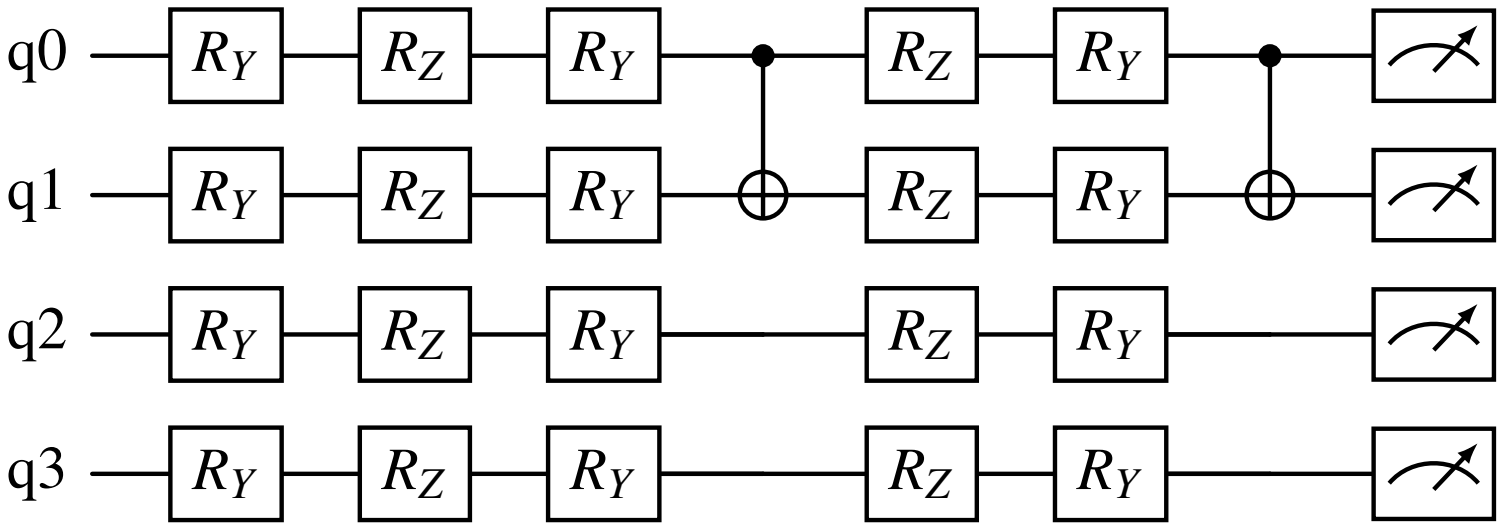

Figure 7: The proposed 4-qubit DV quantum circuit.

Component	**Formula**	**Parameters**	**Description**
Quantum DV Layer	$2 \times 4 \times 4$	32	(R_Y, R_Z, R_Y, R_Z)
Classical Head	$4 \times 2 + 2$	10	Linear layer mapping
Total	–	**42**	Trainable parameters

Discrete-Variable quantum neural network

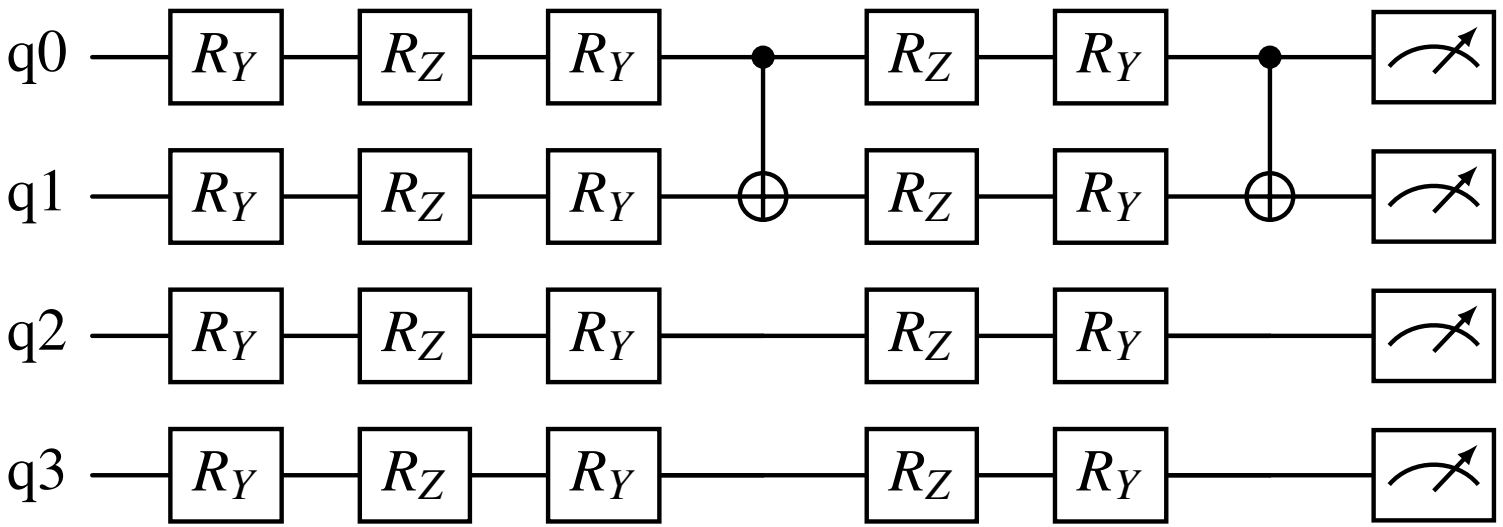

Figure 7: The proposed 4-qubit DV quantum circuit.

Classification Metrics and Confusion Matrix

Classification Metrics

$$P = \frac{TP}{TP + FP},$$

$$R = \frac{TP}{TP + FN},$$

$$ACC = \frac{TP + TN}{TP + TN + FP + FN},$$

$$F1 = 2\left(\frac{P \times R}{P + R}\right). \qquad (10)$$

P: Precision,
R: Recall,
ACC: Accuracy,
F1: F1-score.

Confusion Matrix (Class B)

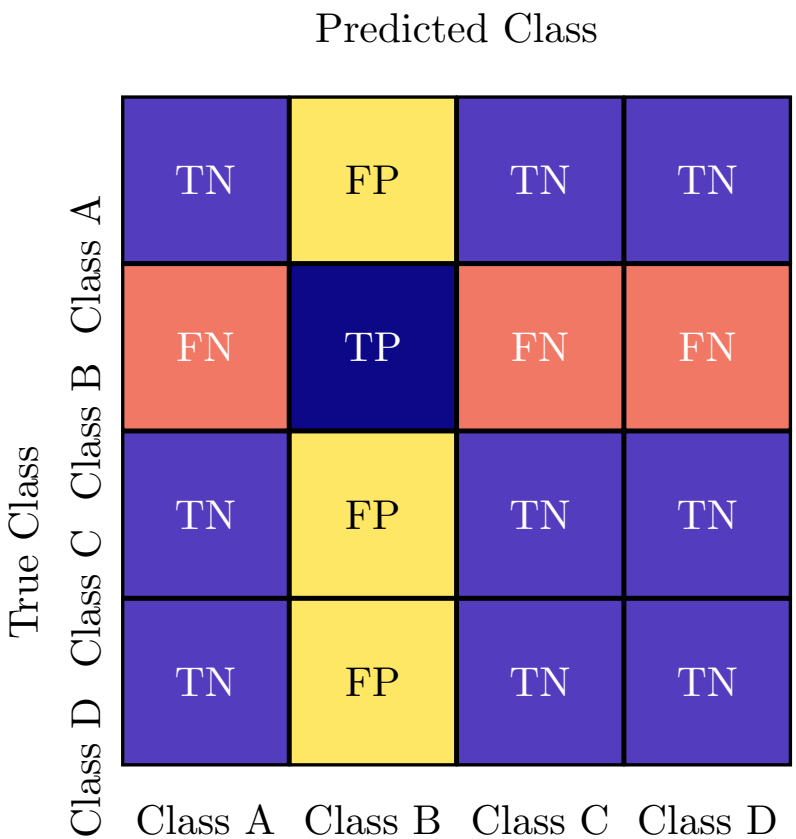

Figure 8: Multiclass confusion matrix for class B.

Area under the characteristic operating curve

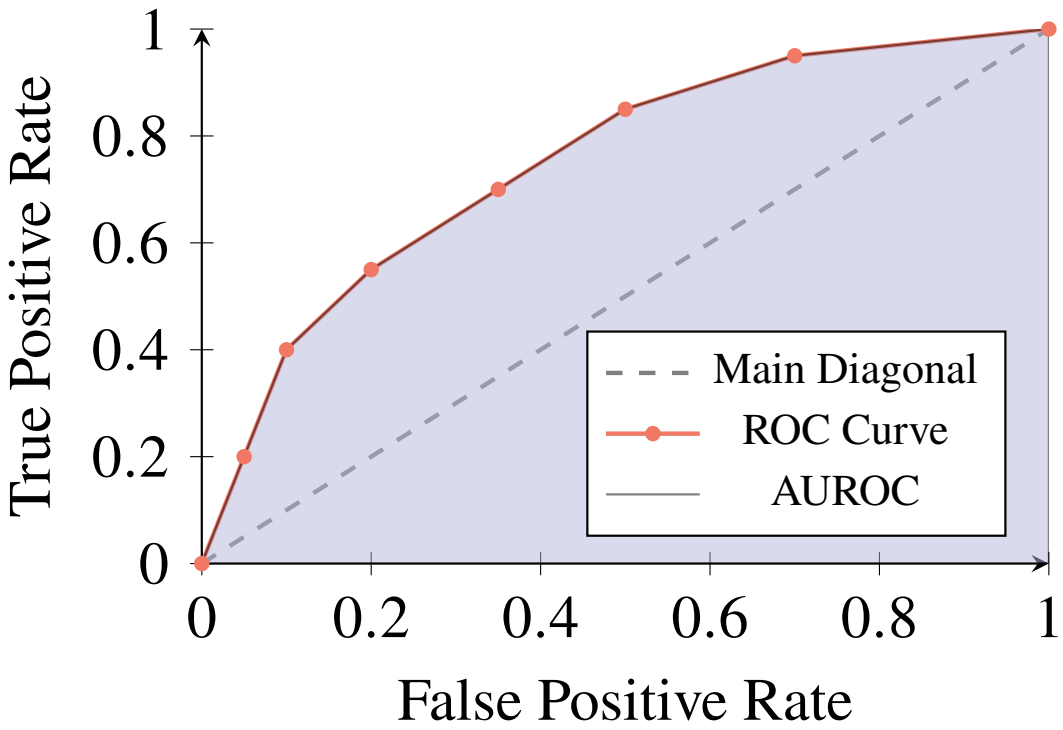

Figure 9: Area under Receiver Operating Characteristic (ROC) curve.

$$AUROC(\sigma) = \int_a^b TPR(\sigma) d(FPR(\sigma). \tag{11}$$

4.- Experiments and results

Classification performance on PneumoniaMNIST

Classification performance on PneumoniaMNIST

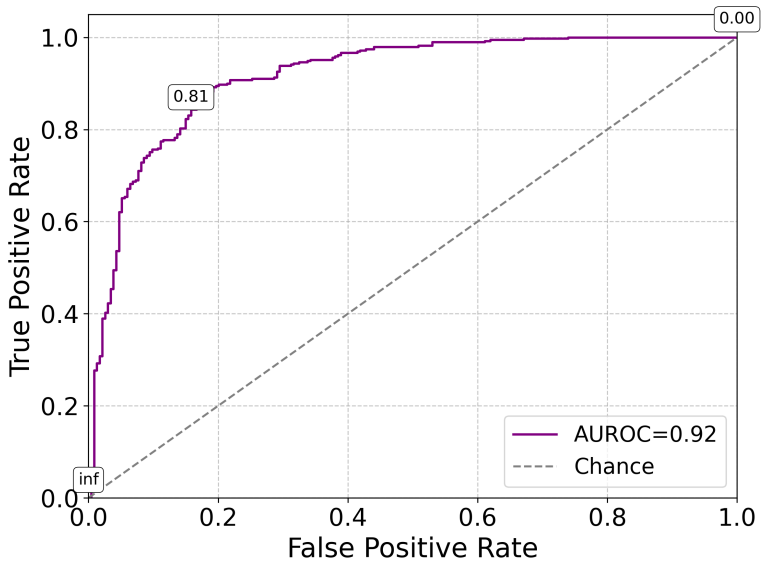

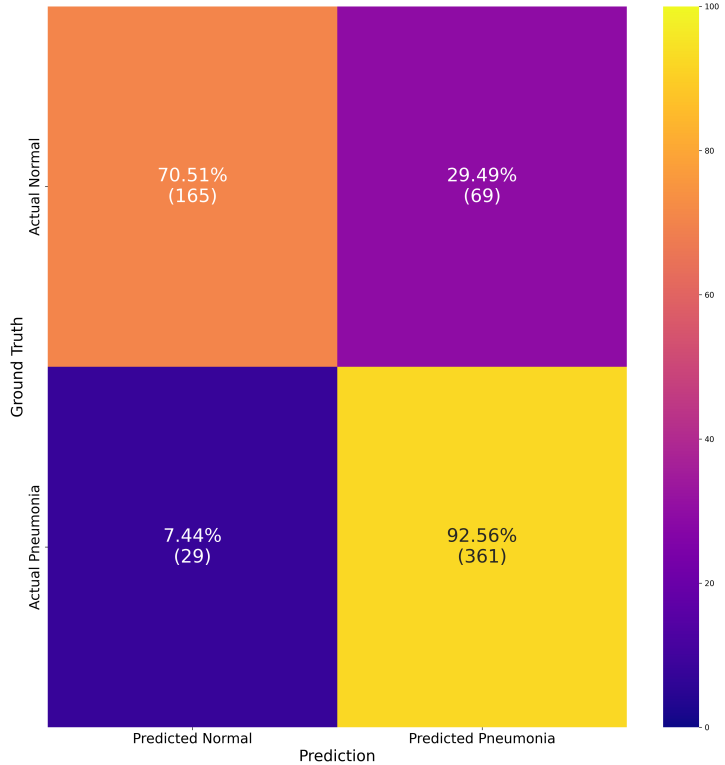

Figure 10: Results for CV QNN on PneumoniaMNIST dataset.

Classification performance on PneumoniaMNIST

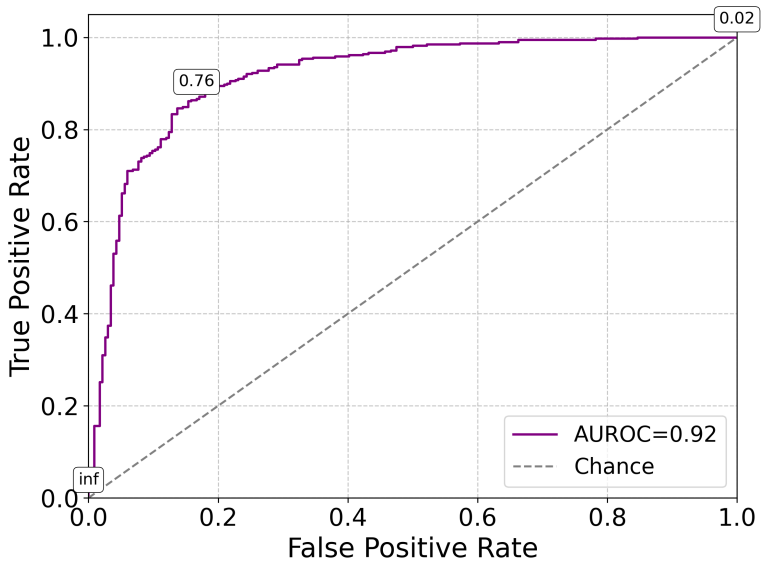

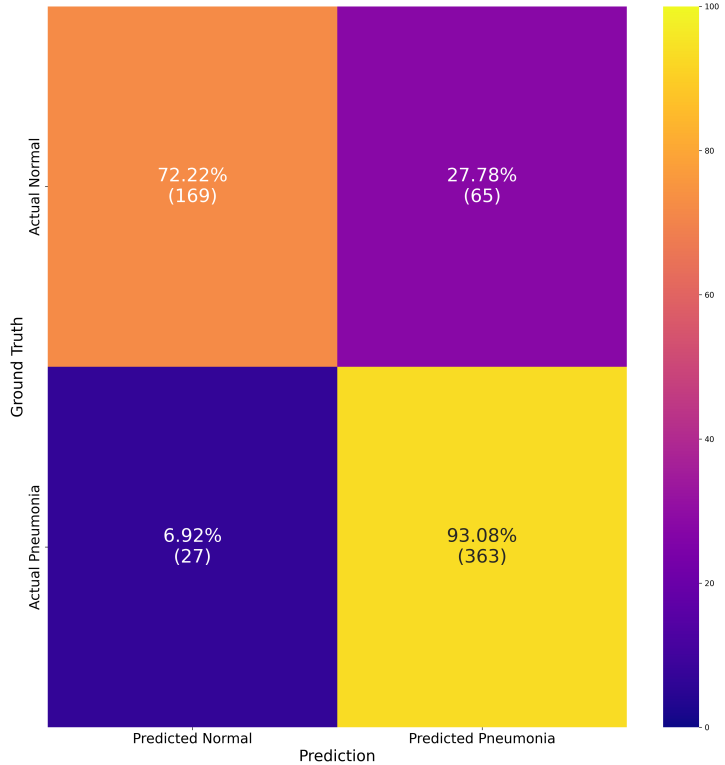

Figure 11: Results for DV QNN on PneumoniaMNIST dataset.

Classification performance on PneumoniaMNIST

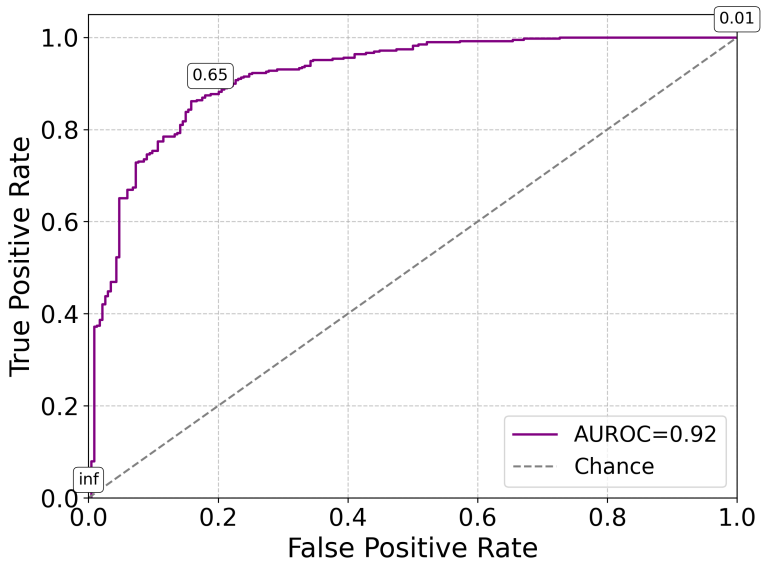

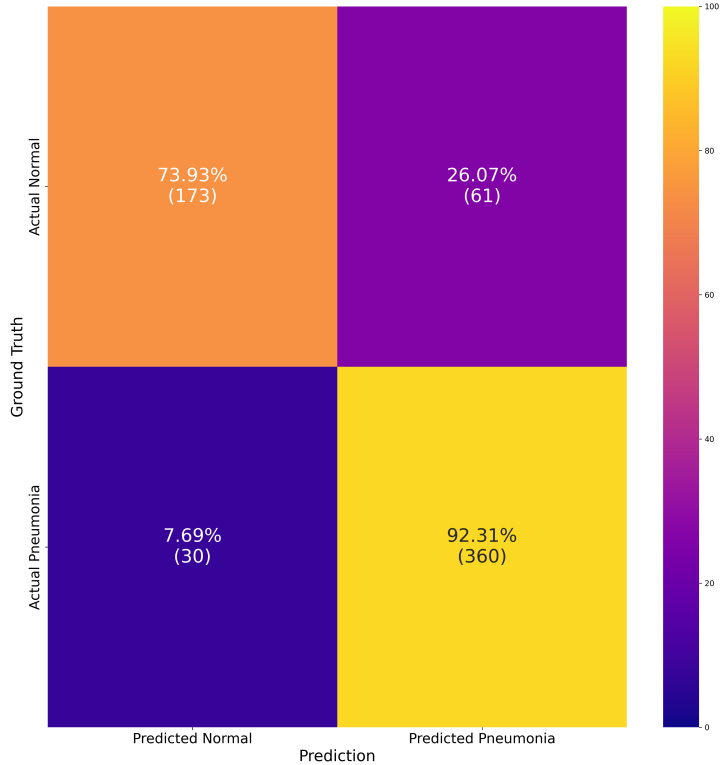

Figure 12: Results for classical NN on PneumoniaMNIST dataset.

Classification performance on OrganAMNIST

Classification performance on OrganAMNIST

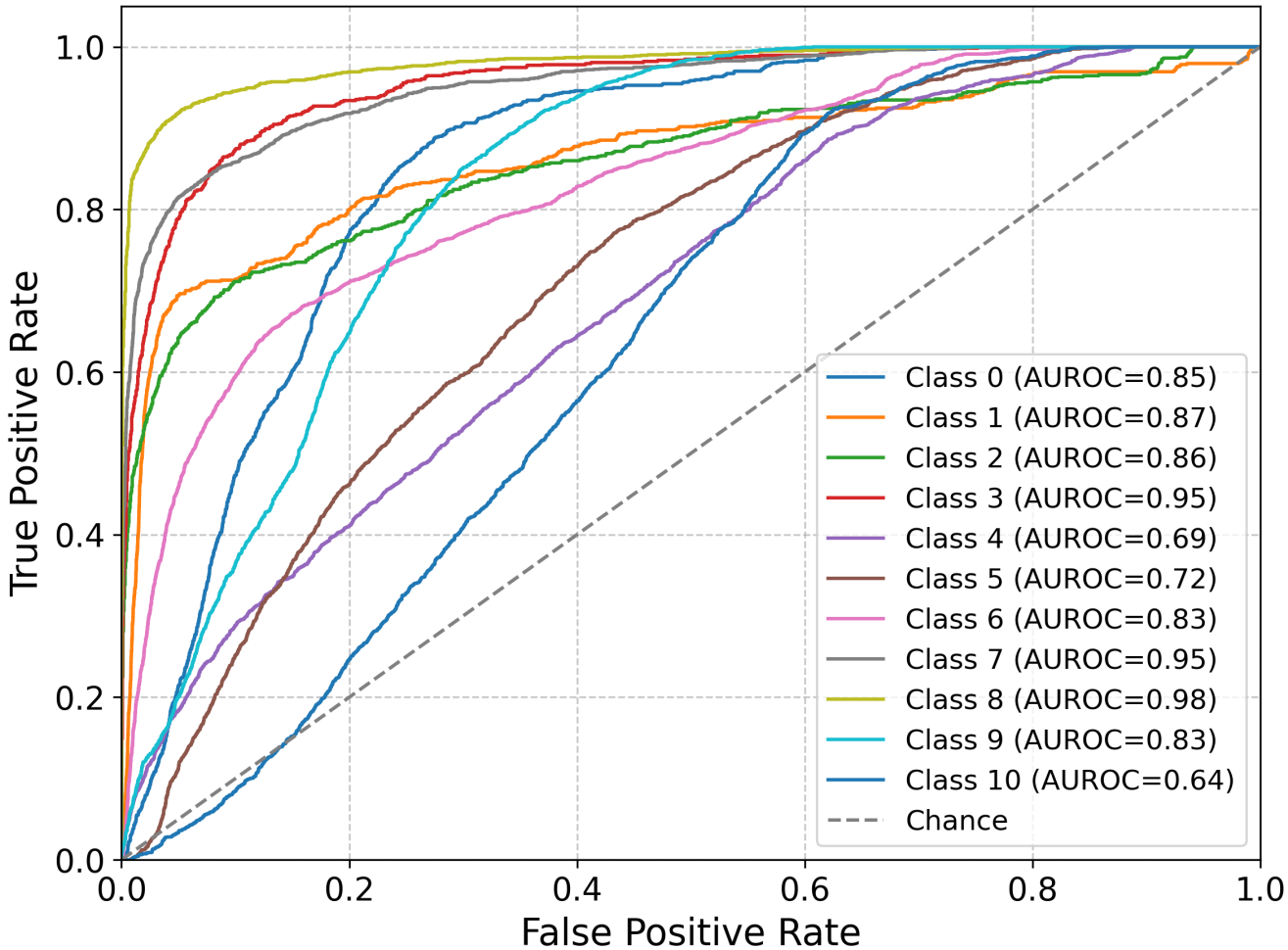

Figure 13: AUROC of CV QNN for OrganAMNIST dataset.

Classification performance on OrganAMNIST

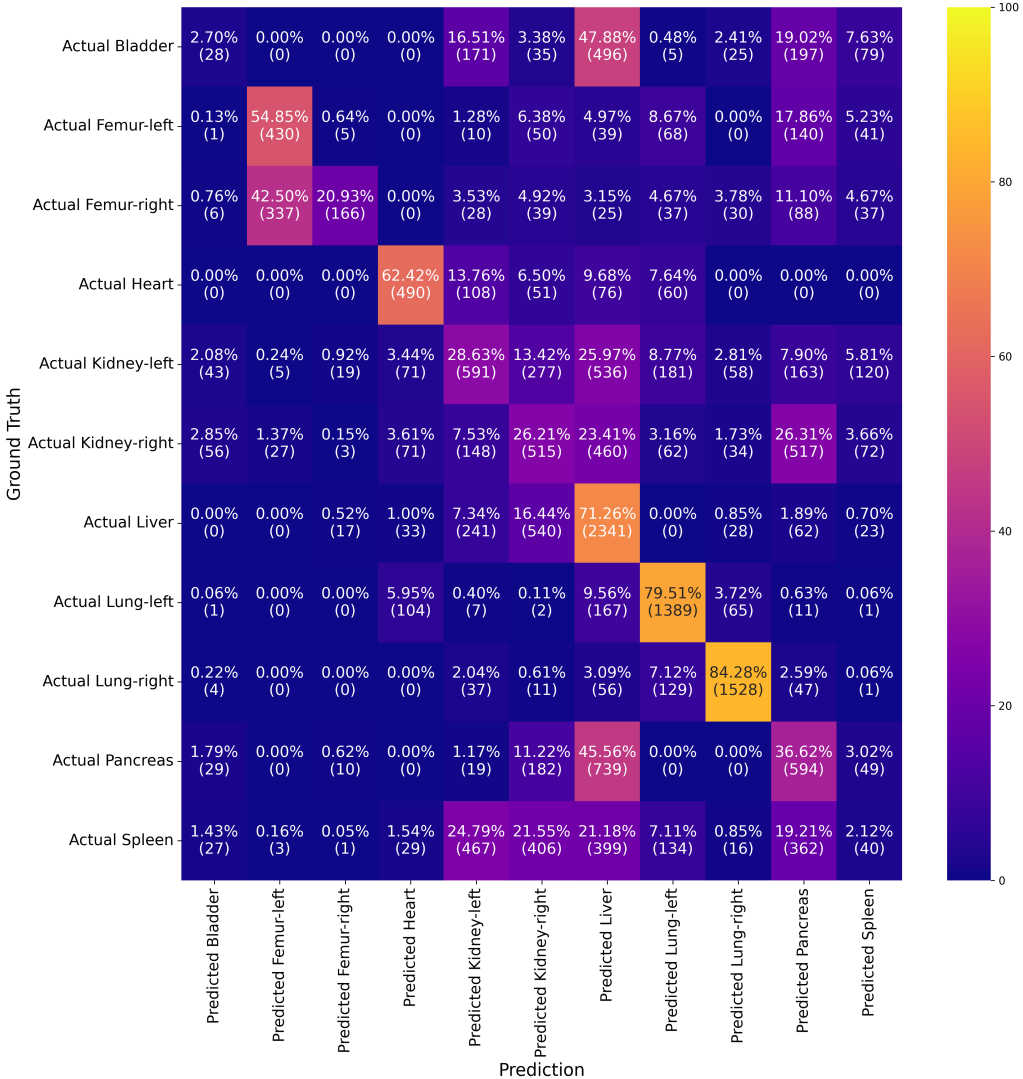

Figure 14: Confusion matrix of CV QNN for OrganAMNIST dataset.

Classification performance on OrganAMNIST

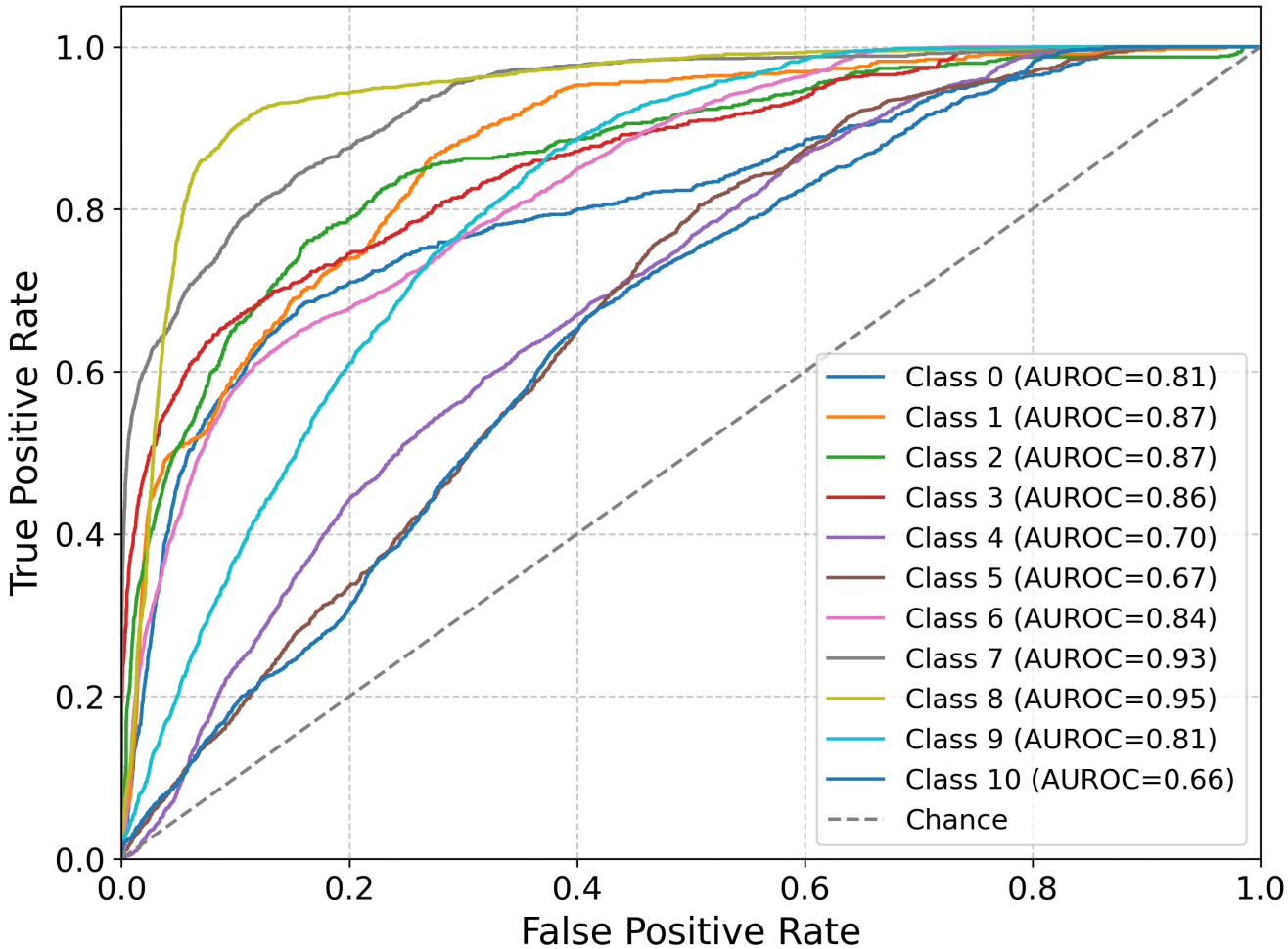

Figure 15: AUROC of DV QNN for OrganAMNIST dataset.

Classification performance on OrganAMNIST

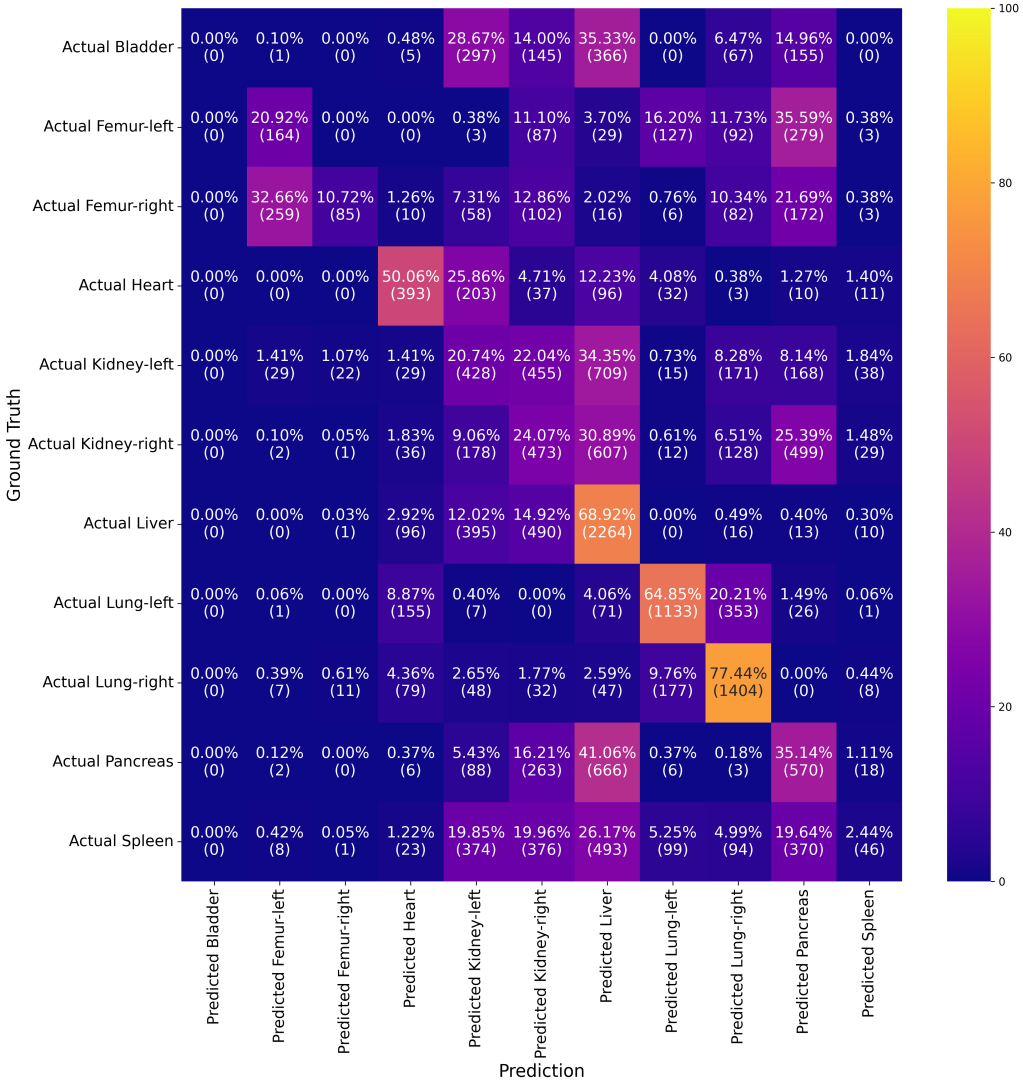

Figure 16: Confusion matrix of DV QNN for OrganAMNIST dataset.

Classification performance on OrganAMNIST

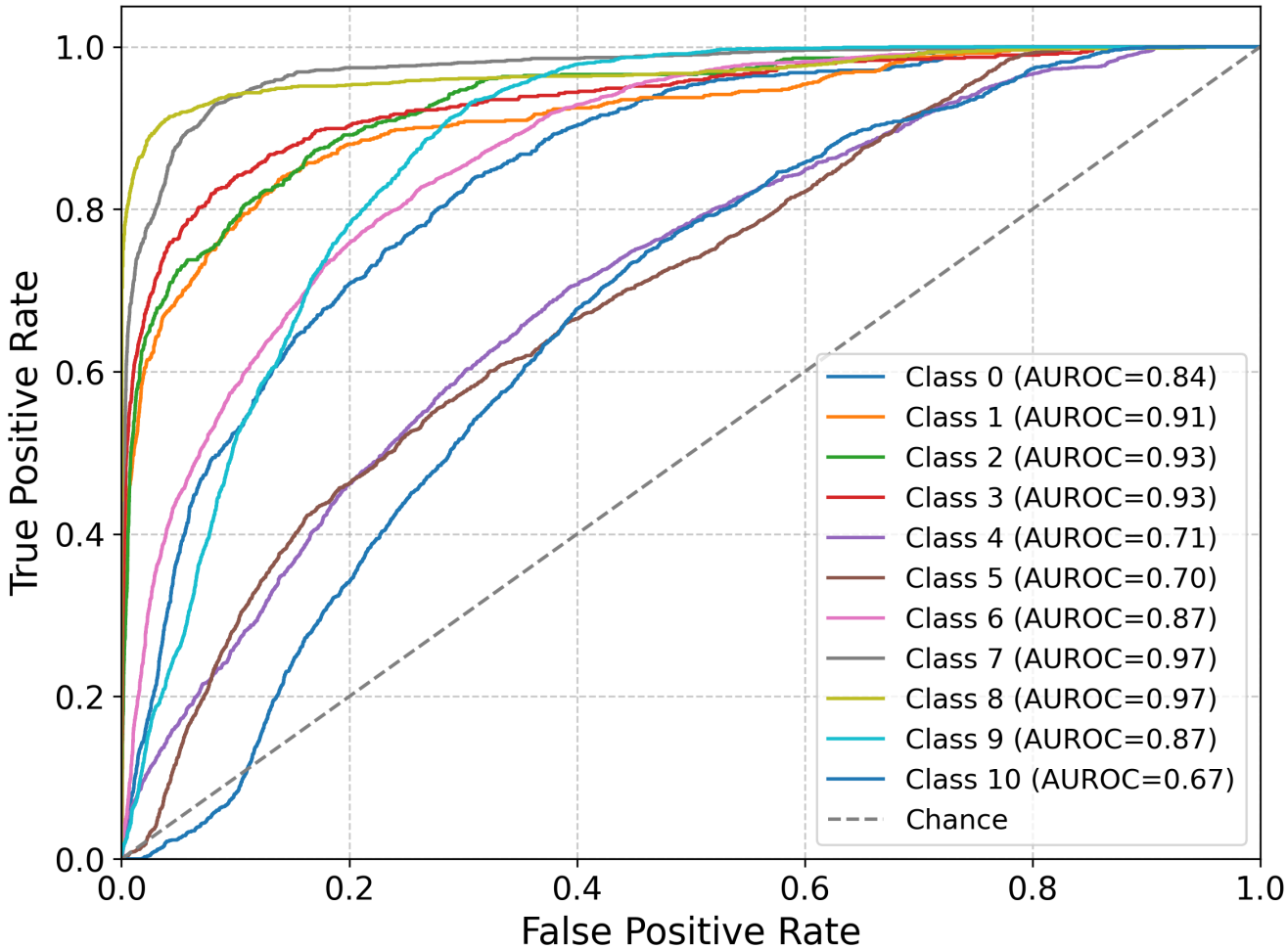

Figure 17: AUROC of classical NN for OrganAMNIST dataset.

Classification performance on OrganAMNIST

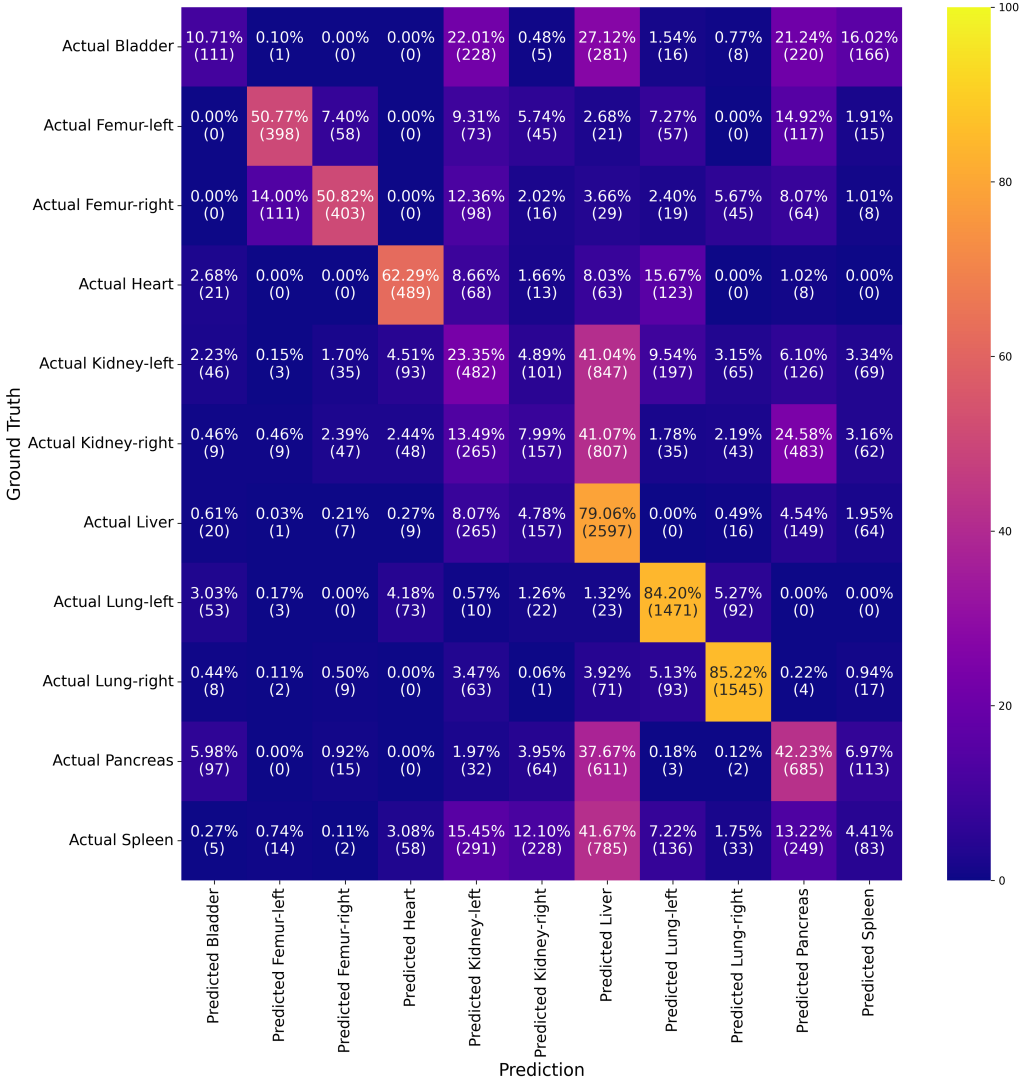

Figure 18: Confusion matrix of classical NN for OrganAMNIST dataset.

Classification performance on BreastMNIST

Classification performance on BreastMNIST

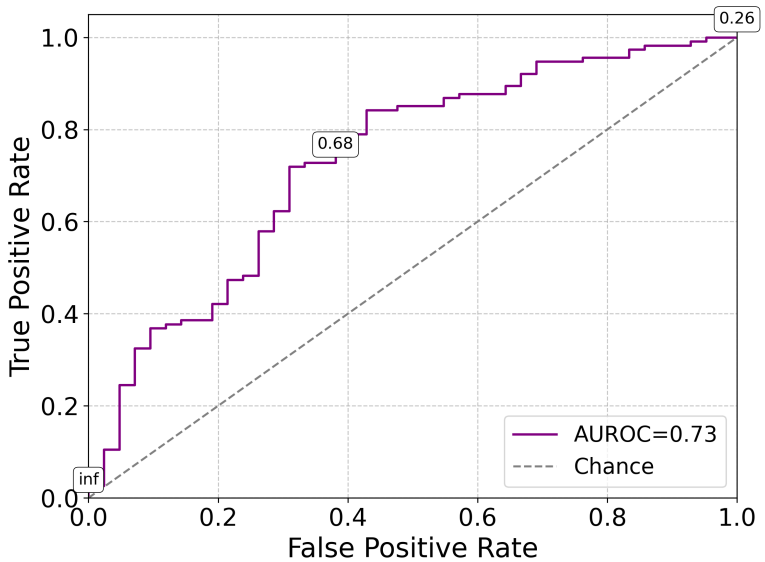

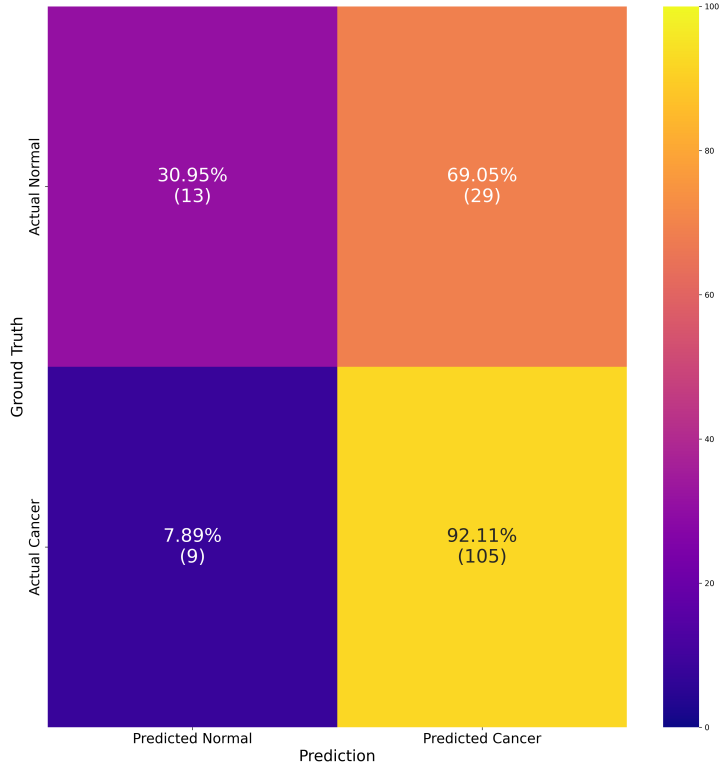

Figure 19: Results for CV QNN on BreastMNIST dataset.

Classification performance on BreastMNIST

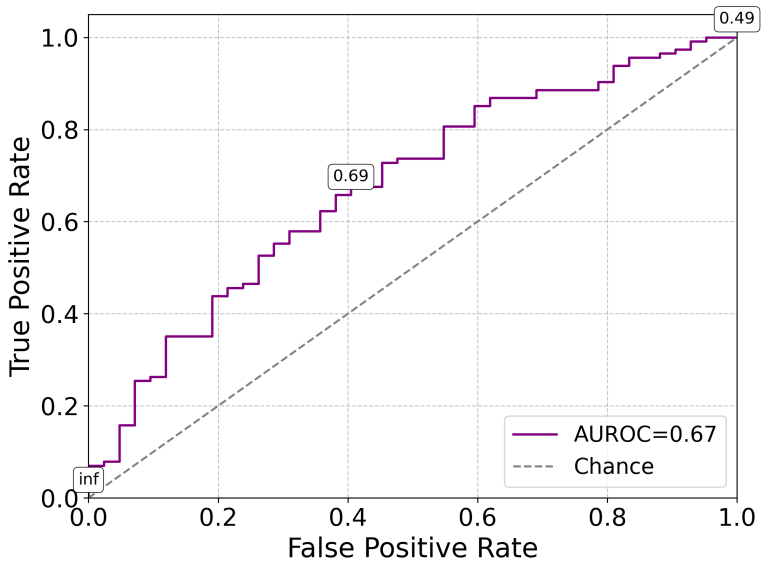

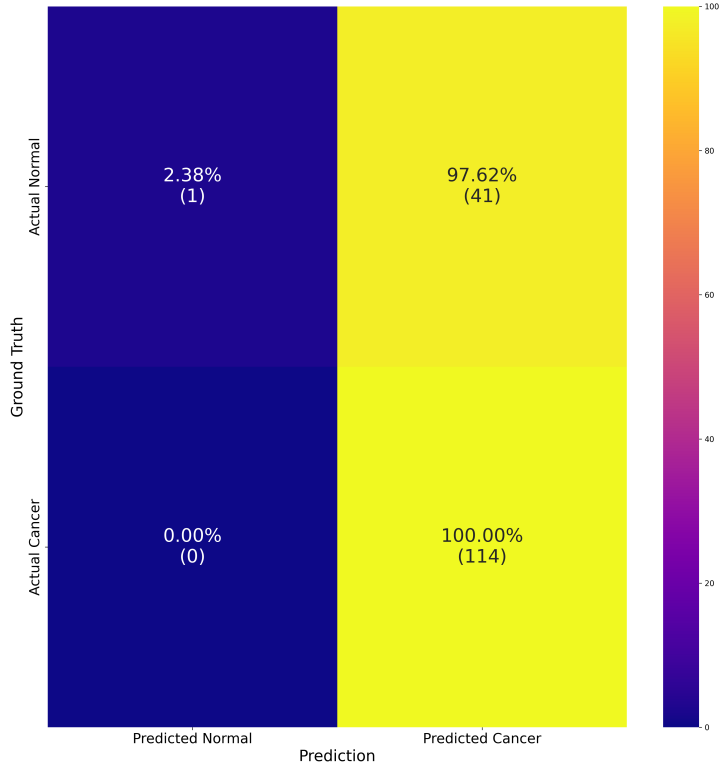

Figure 20: Results for DV QNN on BreastMNIST dataset.

Classification performance on BreastMNIST

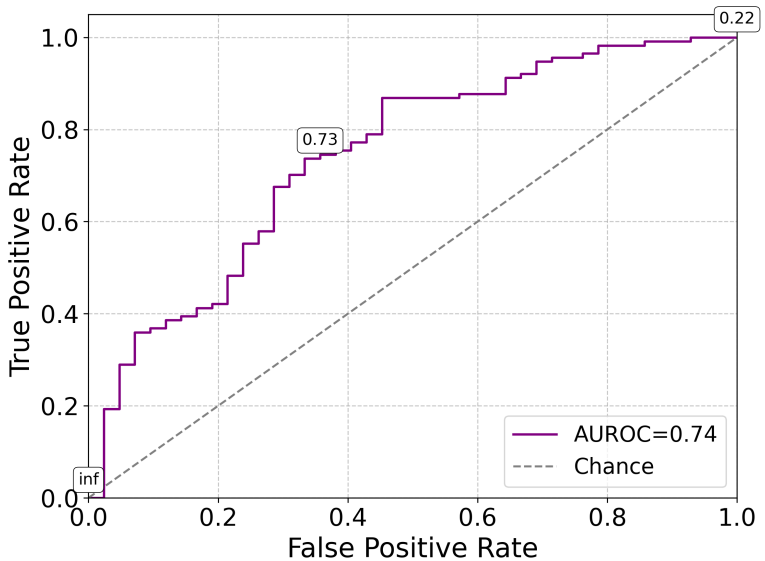

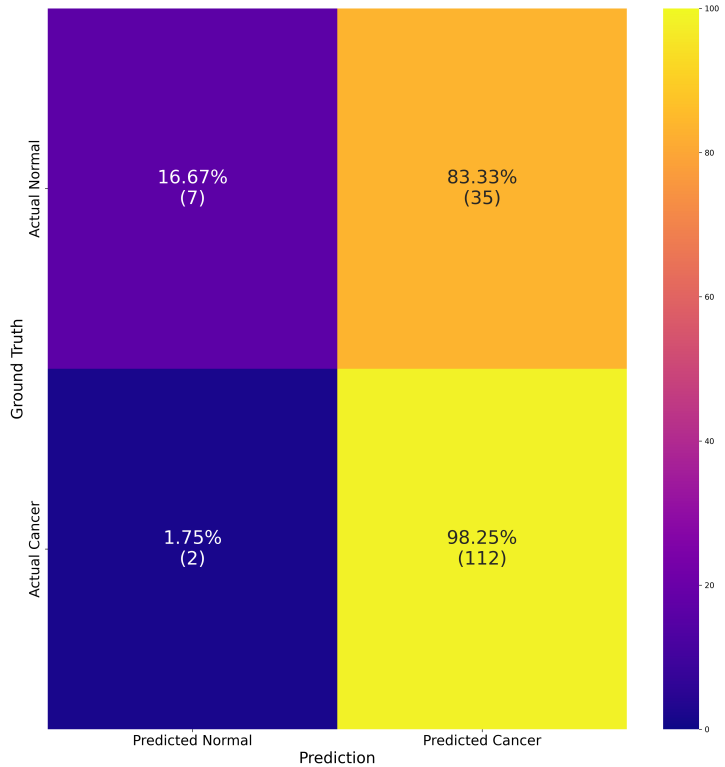

Figure 21: Results for classical NN on BreastMNIST dataset.

Gaussian noise robustness comparison

Gaussian noise robustness comparison

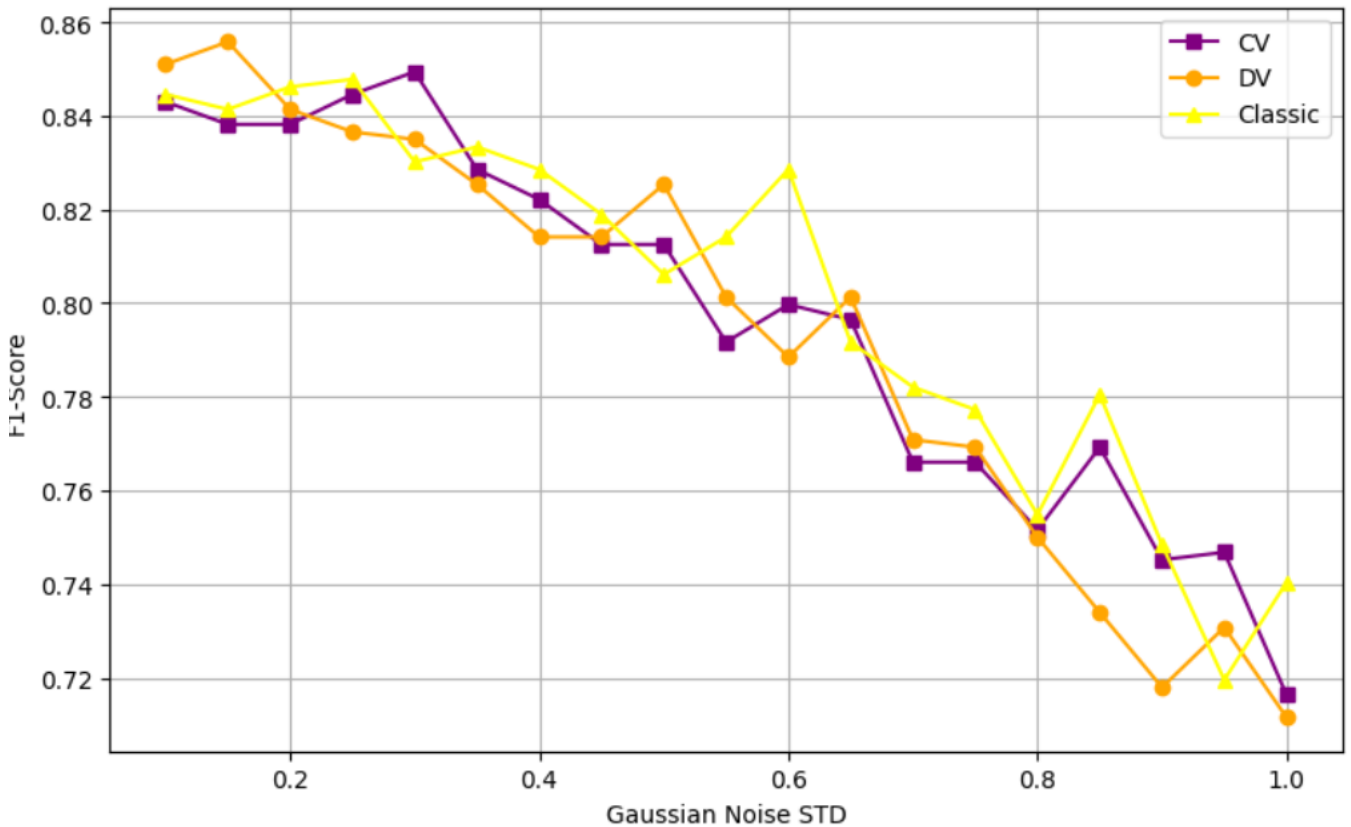

Figure 22: F1 score comparison on Gaussian noise for PneumoniaMNIST dataset.

Gaussian noise robustness comparison

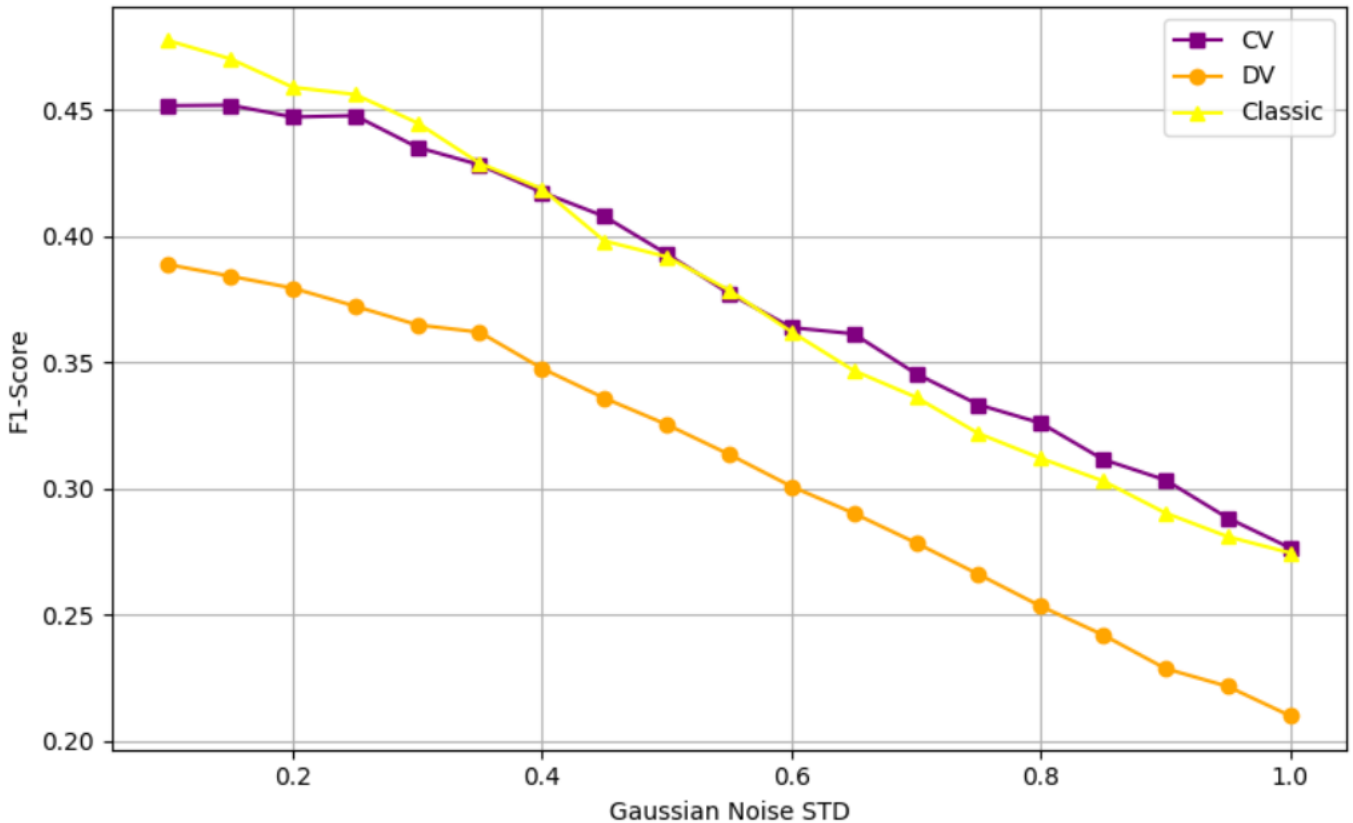

Figure 23: F1 score comparison on Gaussian noise for for OrganAMNIST dataset.

Gaussian noise robustness comparison

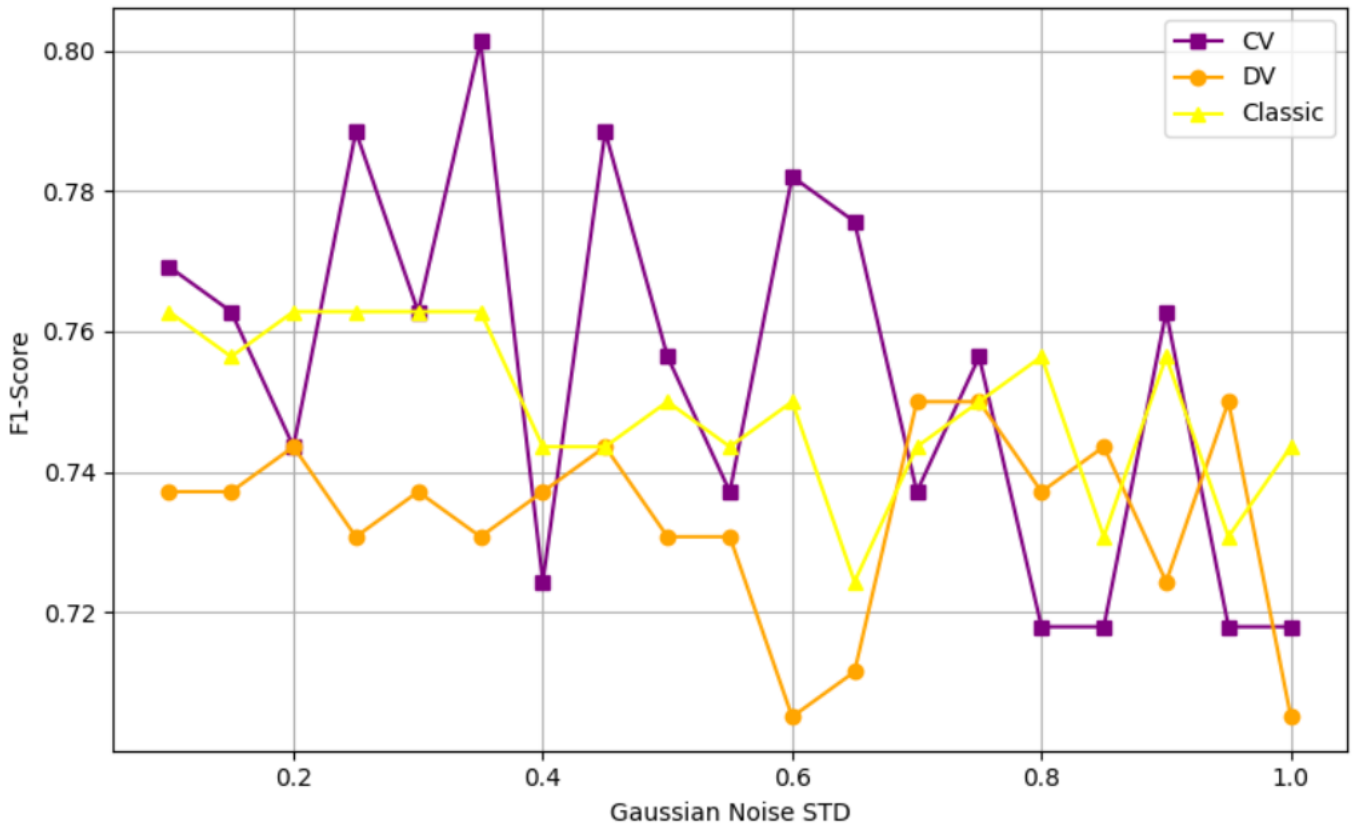

Figure 24: F1 score comparison on Gaussian noise for BreastMNIST.

Test set results summary

Table 2: Test set classification metrics.

Model	Dataset	ACC	P	R	F1	AUROC	AUPRC
CV QNN	BreastMNIST	0.7564	0.7564	0.7317	0.7564	0.73	**0.86**
	OrganAMNIST	0.4563	0.4563	0.4257	0.4563	0.8333	0.4554
	PneumoniaMNIST	0.8429	0.8429	0.8437	0.8429	**0.92**	**0.93**
DV QNN	BreastMNIST	0.7372	0.7372	0.7662	0.7372	0.67	0.84
	OrganAMNIST	0.3915	0.3915	0.3714	0.3915	0.8154	0.3754
	PneumoniaMNIST	**0.8542**	**0.8542**	0.8534	0.8526	**0.92**	**0.93**
Classical	BreastMNIST	**0.7628**	**0.7628**	**0.7662**	**0.7628**	**0.74**	**0.86**
	OrganAMNIST	**0.4737**	**0.4737**	**0.4355**	**0.4737**	**0.8518**	**0.49**
	PneumoniaMNIST	**0.8542**	**0.8542**	**0.8540**	**0.8542**	**0.92**	**0.93**

Decision heatmap comparison

Decision heatmap comparison

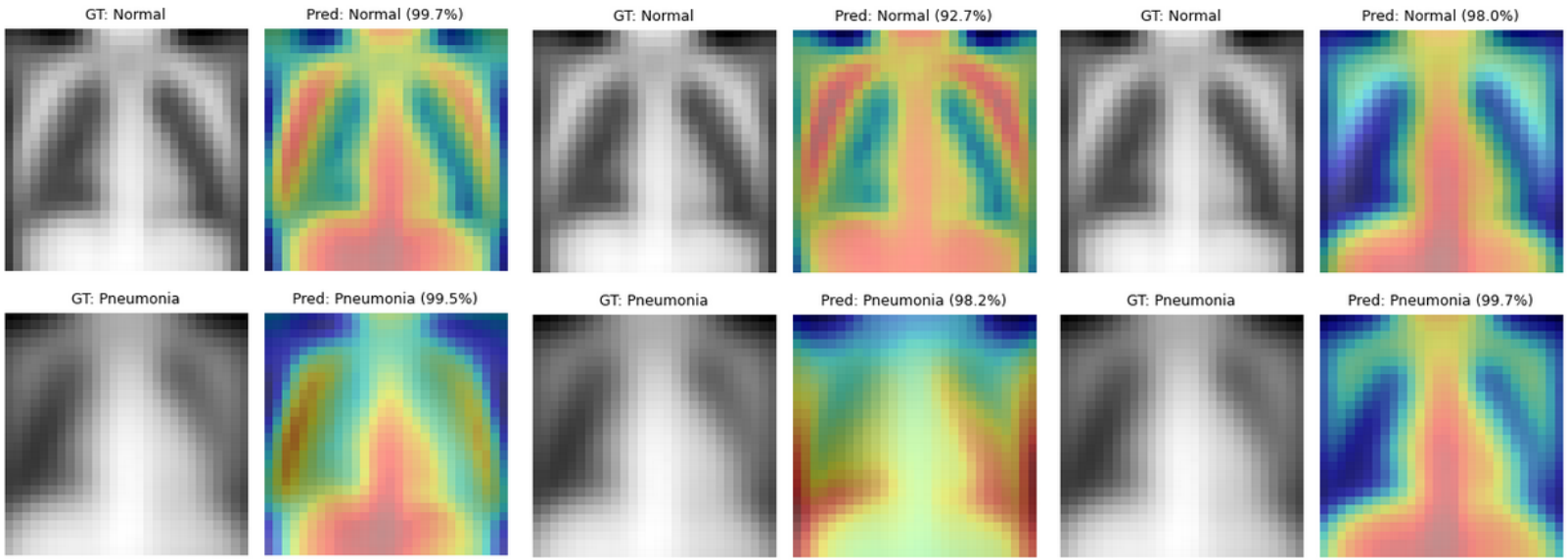

Figure 25: Decision heatmap GradCAM comparison on PneumoniaMNIST.

Decision heatmap comparison

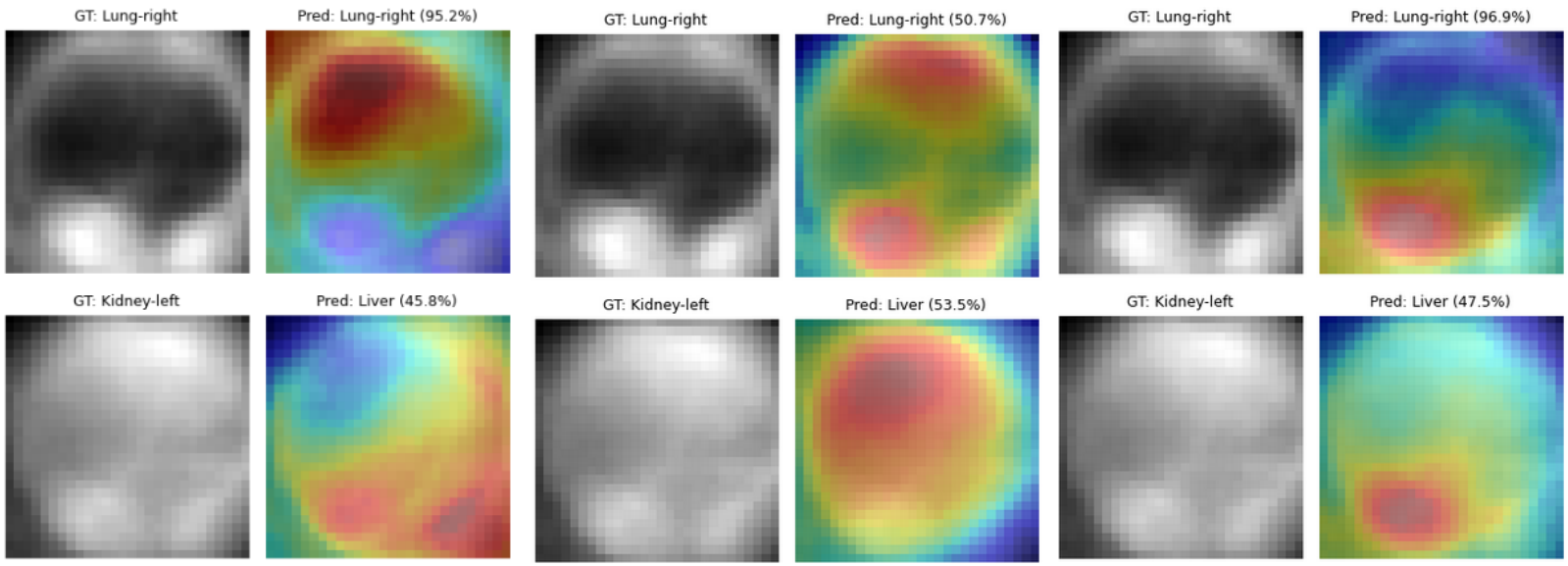

Figure 26: Decision heatmap GradCAM comparison on OrganAMNIST.

Decision heatmap comparison

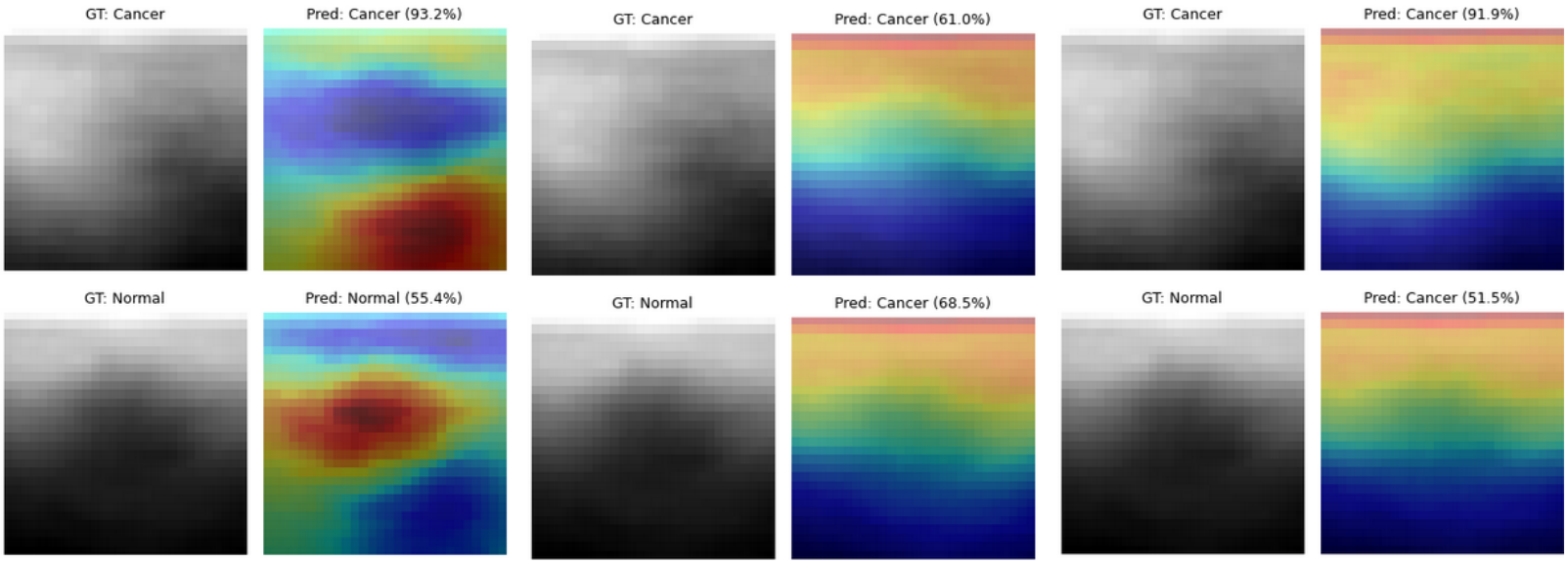

CV QNN DV QNN Classical

Figure 27: Decision heatmap GradCAM comparison.

5.- Conclusions and future work

Conclusions

Conclusions

- The proposed CV and DV quantum models attain **comparable classification performance** to their classical counterpart (F1 scores of 75% in BreastMNIST, 45% OrganAMNIST, 85% in PneumoniaMNIST).

Conclusions

- The proposed CV and DV quantum models attain **comparable classification performance** to their classical counterpart (F1 scores of 75% in BreastMNIST, 45% OrganAMNIST, 85% in PneumoniaMNIST).
- The proposed CV QNN shows slightly **higher performance** than its DV quantum counterpart in **multiclass classification** (+7% F1 score in OrganMNIST), and **slight advantage on minority class** focus (15% TN samples of BreastMNIST).

Conclusions

- The proposed CV and DV quantum models attain **comparable classification performance** to their classical counterpart (F1 scores of 75% in BreastMNIST, 45% OrganAMNIST, 85% in PneumoniaMNIST).
- The proposed CV QNN shows slightly **higher performance** than its DV quantum counterpart in **multiclass classification** (+7% F1 score in OrganMNIST), and **slight advantage on minority class** focus (15% TN samples of BreastMNIST).
- Noise robustness testing shows **high resilience** for the CV QNN, demonstrating stability close to its classical counterpart over different levels of Gaussian noise.

Conclusions

- The proposed CV and DV quantum models attain **comparable classification performance** to their classical counterpart (F1 scores of 75% in BreastMNIST, 45% OrganAMNIST, 85% in PneumoniaMNIST).
- The proposed CV QNN shows slightly **higher performance** than its DV quantum counterpart in **multiclass classification** (+7% F1 score in OrganMNIST), and **slight advantage on minority class** focus (15% TN samples of BreastMNIST).
- Noise robustness testing shows **high resilience** for the CV QNN, demonstrating stability close to its classical counterpart over different levels of Gaussian noise.
- Decision heatmaps of the proposed CV QNN shows **more interpretable highlighted areas**, particularly on the BreastMNIST dataset.

Future work

Future work

- Additional data preparation processes to **maximize data feature representation**.

Future work

- Additional data preparation processes to **maximize data feature representation**.
- Test the proposed quantum models on **more complex datasets**.

Future work

- Additional data preparation processes to **maximize data feature representation**.
- Test the proposed quantum models on **more complex datasets**.
- Further **development on quantum circuit** depth, qumode count, trainable parameters, as well as the introduction of non Gaussian gates.

Presentation references

[1] Andre Esteva et al. 'Dermatologist-level classification of skin cancer with deep neural networks'. In: *Nature* 542 (7639 Feb. 2017), pp. 115–118. ISSN: 1476-4687. DOI: 10.1038/NATURE21056

[2] Constanze Polzer et al. 'AI-based automated detection and stability analysis of traumatic vertebral body fractures on computed tomography'. In: *European Journal of Radiology* 173 (Apr. 2024). ISSN: 18727727. DOI: 10.1016/J.EJRAD.2024.111364

[3] Aqsa Dastgir et al. 'MAFMv3: An automated Multi-Scale Attention-Based Feature Fusion MobileNetv3 for spine lesion classification'. In: *Image and Vision Computing* 155 (Mar. 2025), p. 105440. ISSN: 0262-8856. DOI: 10.1016/J.IMAVIS.2025.105440

[4] Yann Lecun et al. 'Deep learning'. In: *Nature 2015 521:7553* 521 (7553 May 2015), pp. 436–444. ISSN: 1476-4687. DOI: 10.1038/nature14539

[6] Hoi Kwan Lau et al. 'Quantum Machine Learning over Infinite Dimensions'. In: *Physical Review Letters* 118 (8 Feb. 2017), p. 080501. ISSN: 10797114. DOI: 10.1103/PhysRevLett.118.080501

[7] Nathan Killoran et al. 'Continuous-variable quantum neural networks'. In: *Physical Review Research* 1 (3 June 2018). DOI: 10.1103/PhysRevResearch.1.033063

[8] Galan Moody et al. 'Machine learning method for state preparation and gate synthesis on photonic quantum computers'. In: *Quantum Science and Technology* 4 (2 Jan. 2019), p. 024004. ISSN: 2058-9565. DOI: 10.1088/2058-9565/AAF59E

[9] Pranav Kairon and Siddhartha Bhattacharyya. 'COVID-19 Outbreak Prediction Using Quantum Neural Networks'. In: *Advances in Intelligent Systems and Computing* 1279 (2021), pp. 113–123. ISSN: 2194-5365. DOI: 10.1007/978-981-15-9290-4_12

[10] Sophie Choe. 'Continuous Variable Quantum MNIST Classifiers'. In: (Apr. 2022)

[11] Ebrahim Ghasemian et al. 'Quantum machine learning based on continuous variable single-photon states: an elementary foundation for quantum neural networks'. In: *Quantum Information Processing* 22 (10 Oct. 2023), pp. 1–22. ISSN: 15731332. DOI: 10.1007/S11128-023-04137-4/FIGURES/9

[12] Prabhat Anand et al. 'Time-Series Forecasting Using Continuous Variables-Based Quantum Neural Networks'. In: *2024 16th International Conference on COMmunication Systems and NETworkS, COMSNETS 2024* (2024), pp. 994–999. DOI: 10.1109/COMSNETS59351.2024.10427192

Thank you for your attention

dlopez@citedi.mx

Centro de Investigación y Desarrollo de Tecnología Digital (CITEDI-IPN)

Presented at ICE-10 Conference, Valencia, Spain – October 2025